Inorg. Chem. **2006**, *45*, 6282–6297

Influence of the "Innocent" Ligands on the MLCT Excited-State Behavior of Mono(bipyridine)ruthenium(II) Complexes: A Comparison of X-ray Structures and 77 K Luminescence Properties

Yuan-Jang Chen,[†,‡] Puhui Xie,[†] Mary Jane Heeg,[†] and John F. Endicott*[,†]

Department of Chemistry, Wayne State University, Detroit, Michigan 48202-3489, and Department of Chemistry, Fu Jen Catholic University, Taipei Hsien 24205, Taiwan, Republic of China

Received February 14, 2006

The variations in the nonchromophoric ligands of $[Ru(L)_4bpy]^{2+}$ complexes are shown to result in large changes in emission band shapes, even when the emission energies are similar. These changes in band shape are systematically examined by means of the generation of empirical reorganizational energy profiles (emreps) from the observed emission spectra (Xie, P.; et al. *J. Phys. Chem. A* **2005**, *109*, 4671), where these profiles provide convenient probes of the differences in distortions from the ground-state structures of the 2,2-bipyridine (bpy) ligands (for distortion modes near 1500 cm^{-1}) in the metal-to-ligand charge-transfer (MLCT) excited states for a series of complexes with the same ruthenium(II) bipyridine chromophore. The bpy ligand is nearly planar in the X-ray structures of the complexes with $(L)_4 = (NH_3)_4$, triethylenetetraamine (trien), and 1,4,7,10-tetraazacyclododecane ([12]aneN_4). However, for $(L)_4$ = 5,12-*rac*-5,7,7,12,14,14-hexamethyl-1,4,8,11-tetraazacyclotetradecane, the X-ray crystal structure shows that the bpy ligand is twisted in the ground state (a result of methyl/bpy stereochemical repulsion) and the emrep amplitude at about 1500 cm^{-1} is significantly larger for this structure than for the complex with $(L)_4$ = 1,4,8,11-tetraazacyclotetradecane, consistent with larger reorganizational energies of the bpy distortion modes in order to form a planar (bpy^-) moiety in the excited state of the former. The trien and [12]aneN_4 complexes have very nearly the same emission energies, yet the 40% smaller vibronic sideband intensity of the latter indicates that the MLCT excited state is significantly less distorted; this smaller distortion and the related shift in the distribution of distortion mode reorganizational energy amplitudes is apparently related to the 36-fold longer lifetime for $(L)_4$ = [12]aneN_4 than for $(L)_4$ = trien. For the majority (77%) of the $[Ru(L)_4bpy]^{2+}$ complexes examined, there is a systematic decrease in emrep amplitudes near 1500 cm^{-1}, consistent with decreasing excited-state distortion, with the excited-state energy as is expected for ground state–excited state configurational mixing in a simple two-state model. However, the complexes with L = [12]aneN_4, 1,4,7,10-tetraazacyclododeca-1-ene, and $(py)_4$ all have smaller emrep amplitudes and thus less distorted excited states than related complexes with the same emission energy. The observations are not consistent with simple two-state models and seem to require an additional distortion induced by excited state–excited state configurational mixing in most complexes. Because the stereochemical constraints of the coordinated [12]aneN_4 ligand restrict tetragonal distortions around the metal, configurational mixing of the ^{3}MLCT excited state with a triplet ligand-field excited state of Ru^{II} could account for some of the variations in excited-state distortion. The large number of vibrational distortion modes and their small vibrational reorganizational energies in these complexes indicate that a very large number of relaxation channels contribute to the variations in ^{3}MLCT lifetimes and that the metal–ligand skeletal modes are likely to contribute to some of these channels.

Introduction

Ruthenium polypyridine complexes characteristically have reasonably well-defined lowest-energy electronic excited states,[1−3] and these can serve as useful oxidation−reduction reagents and photosensitizers.[3−13] The reactivities of the reagents selected as oxidants or as reductants and the

* To whom correspondence should be addressed. E-mail: jfe@chem.wayne.edu.

[†] Wayne State University.
[‡] Fu Jen Catholic University.

(1) Crosby, G. A. *Acc. Chem. Res.* **1975**, *8*, 231.

10.1021/ic0602547 CCC: $33.50
Published on Web 07/07/2006

efficiencies of the photosensitizers used in various applications are functions of their free energies of reaction, $\Delta G_{RP}°$, electron-transfer reorganizational energies, λ_r, and donor/acceptor (D/A) electronic coupling matrix elements, H_{DA}.[4] However, the relevant oxidation−reduction properties of electronic excited states are usually not directly measurable, so they must be inferred from spectroscopic and/or kinetic measurements (steady-state or transient spectra, excited-state lifetimes, quenching rates, etc.) in combination with some theoretical model. Unfortunately, indirect approaches to the determination of these parameters for transition-metal excited states can be particularly difficult because some of the very properties that give these complexes their high reactivities and their value as catalysts can also complicate the characterization of their excited states: (a) there are frequently a large number of electronic states within a relatively small energy range, as illustrated qualitatively in Figure 1;[14−18] (b) the electronic coupling between some of these states may be relatively large and/or the energy difference between them may be very small, and when this is the case, there will be appreciable configurational mixing among them; (c) the coefficients for the mixing of electronic states will vary as the energy between them varies;[19] (d) the energies of most of the electronic states are functions of the coordination environment of the metal. As a result of these features, the use of the relatively simple two-state theoretical models to obtain electron-transfer parameters may lead to the neglect of such factors as differences in configurational mixings among the excited states in a series of molecules and thus to misleading interpretations of the trends in the inferred electron-transfer parameters.

Many of the important electron-transfer parameters can be obtained spectroscopically; thus, $\Delta G_{RP}° = E^{00\prime} - T\Delta S_{RP}$,

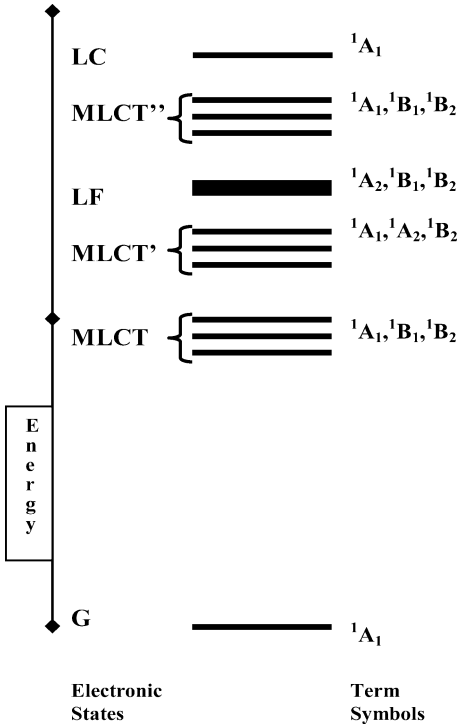

Figure 1. Qualitative energy diagram illustrating the electronic states with singlet spin multiplicity and energies of less than 40 000 cm^{-1} for a typical $[Ru(Am)_4bpy]^{2+}$ complex [Am = an am(m)ine ligand; the energy bar on the left is marked at intervals of approximately 20 000 cm^{-1}]. The electronic states and their approximate energies are based on observations on these or related complexes.[14,16,18,20] Term symbols are based on C_{2v} symmetry; LF = ligand field (dd) excited state of Ru^{II}; LC = ligand centered.

where the energy difference between the potential energy (PE) minima of the ground and electronic excited state is $E^{00\prime}$. The vertical energy differences corresponding to the absorption and emission maxima are $h\nu_{max(abs)} \cong E^{00\prime} + \lambda_{r(e)}$ and $h\nu_{max(em)} \cong E^{0\prime 0} - \lambda_{r(g)}$, respectively, where it is usually assumed that $\lambda_{r(e)} = \lambda_{r(g)} = \lambda_r$. For ruthenium polypyridyl complexes, $E^{00\prime}$ (or $E^{0\prime 0}$) is a dominant component of the absorption (or emission spectrum), and the contributions from the reorganizational energies, λ_r, contribute to the component bandwidth and to the shape of the spectral band in the $[Ru(L)_4bpy]^{2+}$ (where bpy = 2,2-bipyridine) complexes.[12,17,18,21−28] However, extracting the information about either $E^{00\prime}$ or λ_r from the absorption (or $E^{0\prime 0}$ from the emission) spectra of species in ambient solutions is complicated by intrinsically large bandwidths, and the band-shape analysis of the absorption spectra is often further complicated

(2) Yersin, H.; Braun, D.; Hensler, G.; Galhuber, E. In *Vibronic Processes in Inorganic Chemistry*; Flint, C. D., Ed.; Kluwer: Dordrecht, The Netherlands, 1989; p 195.
(3) Kalyanasundaram, K. *Photochemistry of Polypyridine and Porphyrin Complexes*; Academic Press: New York, 1992.
(4) *Electron Transfer in Chemistry*; Balzani, V., Ed.; Wiley-VCH: Weinheim, Germany, 2001; Vols. 1−5.
(5) Cannon, R. D. *Electron-Transfer Reactions*; Butterworth: London, 1980.
(6) Ferraudi, G. J. *Elements of Inorganic Photochemistry*; Wiley: New York, 1988.
(7) Sutin, N. *Acc. Chem. Res.* **1982**, *15*, 275.
(8) Sutin, N. *Prog. Inorg. Chem.* **1983**, *30*, 441.
(9) Meyer, T. J.; Taube, H. In *Comprehensive Coordination Chemistry*; Wilkinson, G., Gillard, R. D., McCleverty, J., Eds.; Pergamon: Oxford, England, 1987; Vol. 7; p 331.
(10) Juris, A.; Balzani, V.; Barigelletti, F.; Compagna, S.; Belser, P. L.; von Zelewsky, A. *Coord. Chem. Rev.* **1988**, *84*, 85.
(11) Gratzel, M. *Heterogeneous Photochemical Electron Transfer*; CRC Press: Boca Raton, FL, 1989.
(12) Barbara, P. F.; Meyer, T. J.; Ratner, M. *J. Phys. Chem.* **1996**, *100*, 13148.
(13) Gratzel, M.; Moser, J.-E. In *Electron Transfer in Chemistry*; Balzani, V., Ed.; Wiley-VCH: Weinheim, Germany, 2001; Vol. 5; p 589.
(14) Lever, A. B. P. *Inorganic Electronic Spectroscopy*; Elsevier: Amsterdam, The Netherlands, 1984.
(15) Lever, A. B. P.; Gorelsky, S. I. *Coord. Chem. Rev.* **2000**, *208*, 153.
(16) Lever, A. B. P.; Gorelsky, S. I. *Struct. Bonding* **2004**, *107*, 77.
(17) Seneviratne, D. S.; Uddin, M. J.; Swayambunathan, V.; Schlegel, H. B.; Endicott, J. F. *Inorg. Chem.* **2002**, *41*, 1502.
(18) Endicott, J. F.; Uddin, M. J.; Schlegel, H. B. *Res. Chem. Intermed.* **2002**, *28*, 761.
(19) Mulliken, R. S.; Person, W. B. *Molecular Complexes*; Wiley-Interscience: New York, 1967.
(20) Hakamata, K.; Urushiyama, A.; Kupka, H. *J. Phys. Chem.* **1981**, *85*, 1983.
(21) Hush, N. S. *Prog. Inorg. Chem.* **1967**, *8*, 391.
(22) Hush, N. S. *Electrochim. Acta* **1968**, *13*, 1005.
(23) Gould, I. R.; Noukakis, D.; Gomez-Jahn, L.; Young, R. H.; Goodman, J. L.; Farid, S. *Chem. Phys.* **1993**, *176*, 439.
(24) Graff, D.; Claude, J. P.; Meyer, T. J. In *Electron-Transfer Reactions: Inorganic, Organometallic and Biological Applications*; Isied, S. S., Ed.; American Chemical Society: Washington, DC, 1997; p 183.
(25) Endicott, J. F.; Uddin, M. J. *Coord. Chem. Rev.* **2001**, *219−221*, 687.
(26) Endicott, J. F. In *Comprehensive Coordination Chemistry II*, 2nd ed.; McCleverty, J., Meyer, T. J., Eds.; Pergamon: Oxford, U.K., 2003; Vol. 7; p 657.
(27) Endicott, J. F.; Chen, Y.-J.; Xie, P. *Coord. Chem. Rev.* **2005**, *249*, 343.
(28) Xie, P.; Chen, Y.-J.; Uddin, M. J.; Endicott, J. F. *J. Phys. Chem. A* **2005**, *109*, 4671.

by the overlapping contributions of different electronic transitions. On the other hand, transition-metal complex emission spectra generally correspond to a single electronic transition of the lowest-energy electronic excited state,[2,28−31] and approaches have recently evolved for evaluating the variations of electron-transfer parameters within a series of closely related complexes by means of the careful comparison of the shapes of the relatively broad band 77 K emission spectra of $[Ru(Am)_{6-2n}(bpy)_n]^{2+}$ complexes in frozen solutions.[27,28,32] The analysis of the band shapes of these complexes is facilitated by removing from the experimental spectrum the dominant contribution of the fundamental component, which corresponds to the {e, 0′} → {g, 0} transition, $I_{max(f)}$, and comparing either (a) the difference spectra, $I_{\nu_m(diff)}$, which correspond to the sums of the spectral intensities of the components of all of the vibronic progressions, or (b) a reorganizational energy profile constructed by multiplying the normalized difference spectrum, $I_{\nu_m(diff)} \div I_{max(f)}$, by the spectral frequency difference from the fundamental (with a generally small correction for the non-Gaussian shapes of the vibrational reorganizational energy contributions) to obtain a profile whose amplitude varies as the sum of the overlapping reorganizational energy contributions of the displacement modes.[27,28,32−34] The latter approach is the most sensitive to variations in the reorganizational energies in a series of complexes because $I_{\nu_m(diff)}$ does not directly reflect variations in the electron-transfer reorganizational energies. Thus, the intensity contributions to the emission or difference spectrum of each of the first-order components in the vibronic progressions are given by[35,36]

$$I_{max(k)} = (\lambda_k/h\nu_k)I_{max(f)} \quad (1)$$

A more direct measure of the reorganizational energy information can be based on rearranging eq 1, or

$$\lambda_k = h\nu_k(I_{max(k)}/I_{max(f)}) \quad (2)$$

Information about electron-transfer reorganizational energies can be inferred from absorption and/or emission band shapes because the convolution of the sums of vibronic progressions in the distortion modes results in broad shoulders and/or weak peaks on the high-energy sides of the absorption and low-energy sides of the emission band maxima in $[Ru(Am)_4bpy]^{2+}$ complexes.

The Ru−bpy charge-transfer processes of a series of closely related $[Ru(L)_4bpy]^{2+}$ complexes in solution are most simply treated in terms of the Ru−bpy chromophore, with variations of the $(L)_4$ ligands providing a means for changing the excited-state energies, $E_{ge}^{00'}$. Because the electronic matrix elements are large for these complexes ($H_{ge} \sim 7 \times 10^3$ cm^{-1}),[17] configurational mixing with the ground state will (a) increase $E_{ge}^{00'}$ by approximately $2\epsilon_{ge} \cong 2H_{ge}^2/(E_{ge}^{00'} + \lambda_r)$[19] and (b) decrease the reorganizational energy, λ_r, because the configurational mixing shifts the PE minima nearer to one another (see Figure 2), so that for $\alpha_{jk}^2 < 0.1$ and identical ground- and excited-state force constants[17,27,28,37]

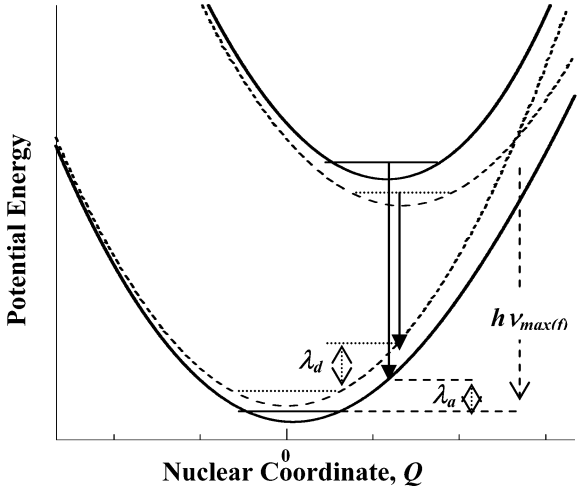

Figure 2. PE curves qualitatively illustrating the effects of configurational mixing on the reorganizational energy, λ_r (r = a for adiabatic and r = d for diabatic): $\lambda_a < \lambda_d$.

$$\lambda_r \cong \lambda_r^{\circ}(1 - 2\alpha_{ge}^2 - 2\alpha_{eg}^2) \quad (3)$$

In this expression, λ_r is the reorganizational energy of any distortion coordinate, $\alpha_{ge} = H_{ge}/E_{ge}(1 + H_{ge}^2/E_{ge}^2)^{-1/2}$ is the normalized mixing coefficient, $E_{ge} = (E_{ge}^{00'} + \lambda_r)$ is the vertical energy difference between the ground and excited states evaluated at the nuclear coordinates of the ground-state PE, minimum, α_{eg} is the mixing coefficient evaluated at the excited-state PE minimum, and the degree symbol designates the value of the parameter in the absence of configurational mixing. The decreases of excited-state distortion with increases of ground state−excited state configurational mixing, illustrated in eq 3 and Figure 2, account for much of the attenuation of the vibronic structure that accompanies the decreases of emission energies in the $[Ru(Am)_{6-2n}(bpy)_n]^{2+}$ complexes;[28,38] however, configurational mixing among the excited states could alter the simple pattern, and the more shallow attenuation of the vibronic structure with decreasing emission energy observed[28] for the tetraam(m)ine complexes than expected in comparisons based on eq 3 could be a consequence of mixing among the excited states.[28]

In order for an emission to be observed, $E^{00'} \gg \lambda_r$, and the nonradiative relaxation of the excited state corresponds to electron transfer in the Marcus inverted region. The

(29) This may be complicated by the thermal population spin−orbit states of the excited state;[2] however, the excellent fits of the rR parameters[31,32] to the 77 K emission spectra of $[Ru(NH_3)_4bpy]^{2+}$ and $[Ru(bpy)_3]^{2+}$ [28] indicate that this is not a major issue.

(30) Maruszewski, K.; Bajdor, K.; Strommen, D. P.; Kincaid, J. R. *J. Phys. Chem.* **1995**, *99*, 6286.
(31) Hupp, J. T.; Williams, R. T. *Acc. Chem. Res.* **2001**, *34*, 808.
(32) Chen, Y.-J.; Xie, P.; Endicott, J. F. *J. Phys. Chem. A* **2004**, *108*, 5041.
(33) Chen, Y.-J.; Xie, P.; Endicott, J. F.; Odongo, O. S. *J. Phys. Chem. A* **2006**, *110*, 7970.
(34) Chen, Y.-J.; Endicott, J. F.; Swayambunathan, V. *Chem. Phys.* **2006**, *326*, 79.
(35) Solomon, E. I. *Comments Inorg. Chem.* **1984**, *3*, 225.
(36) Brunold, T. C.; Gudel, H. U. In *Inorganic Electronic Structure and Spectroscopy*; Solomon, E. I., Lever, A. B. P., Eds.; Wiley-Interscience: New York, 1999; Vol. 1; p 259.
(37) Endicott, J. F.; Schegel, H. B.; Uddin, M. J.; Seneviratne, D. *Coord. Chem. Rev.* **2002**, *229*, 95.
(38) Xie, P.; Chen, Y.-J.; Endicott, J. F.; Uddin, M. J.; Seneviratne, D.; McNamara, P. G. *Inorg. Chem.* **2003**, *42*, 5040.

patterns of reactivity for the nonradiative electron-transfer processes that transform reactants into products are generally determined by the accompanying changes in their internuclear distances and angles; the squares of the corresponding displacements in nuclear coordinates are generally expressed in terms of vibrational reorganizational energies (λ_h). Thus, most theoretical models predict that the inverted-region reaction channels are dominated by the highest-frequency vibrational modes for which the nuclear distortions are significant.[39−42] Furthermore, because $k_BT \cong 53\ cm^{-1}$ at 77 K, the condition that $E^{00\prime} \gg \lambda_r$ indicates that the electron-transfer processes that correlate with the emission are in the low-temperature, or nuclear tunneling limit. For a two-state system that is distorted in a single vibrational mode (ν_h), the electron-transfer rate constant in this limit can be described as[39]

$$(k_{nr}^{\circ})_h \cong H_{eg}{}^2\left[\frac{8\pi^3}{h^3\nu_h E^{0'0}}\right]^{1/2} e^{-\gamma_h(E^{0\prime 0}/h\nu_h)}, \quad \gamma_h = \ln\left(\frac{E^{0,0}}{\lambda_h}\right) - 1 \tag{4}$$

Although the highest-frequency vibrational modes are the C−H and/or N−H stretching modes in the complexes considered here, the rates of polypyridyl (PP) complex metal-to-ligand charge-transfer (MLCT) excited-state electron transfer and/or nonradiative relaxation are often adequately described in terms of the displacements in the skeletal modes of the PP ligands of the M−PP chromophore[12,24,28,43−46] rather than the higher-frequency stretching modes. This might be related to observations that the squared displacements (and the corresponding vibrational reorganizational energies, λ_h) of some of the bpy skeletal modes[30,31] are more than 10 times larger than those of the R−H stretching modes.[33] However, resonance Raman (rR) studies indicate that the MLCT excited-state distortions of Ru−bpy complexes involve at least 11 vibrational modes with frequencies of less than 1650 cm^{-1},[30,31] all with $\lambda_h < 300\ cm^{-1}$; the substitution of the observed parameters into eq 4 indicates that no single distortion mode can account for more than about 0.01% of the observed rate constants[28] and, thus, that relaxation rate constants, k_{nr}, should be interpreted in terms of the sum over h relaxation channels, each corresponding to a different combination of the distortion modes such that $(E_{ge}{}^{00\prime} \pm k_BT)_h \cong h(a_1\nu_1 + a_2\nu_2 + a_3\nu_3 + ...)$.[27,28] Furthermore, the rR studies[30,31] and the RH/RD isotope effects combined with the spectroscopic effects of ligand deuteration of the $[Ru(Am)_{6-2n}(bpy)_n]^{2+}$ complexes (Am = an am(m)ine ligand)[33] have implicated contributions of the even lower-frequency metal−ligand skeletal modes in the dominant relaxation channels of these complexes. The variations of the "innocent" ligands $(L)_4$ in $[Ru(L)_4bpy]^{2+}$ complexes are expected to alter the excited-state energies, but the above considerations suggest that their variation might also be used to manipulate the effective electron-transfer reorganizational energies and the contributions to relaxation channels with mixed-mode character. This report describes the appreciable changes in the Ru−bpy MLCT excited-state emission spectra and lifetimes that result when these "innocent" ligands are altered.

We have now synthesized and characterized an extensive series of mono(bipyridine) complexes in order to examine the issues outlined above.

Experimental Section

1. Materials and Synthesis of Compounds. The ligands 2,2-bipyridine (bpy), ethylenediamine (en), triethylenetetramine (trien), and 1,4,7,10-tetraazacyclododecane ([12]aneN$_4$ or cyclen) were purchased from Aldrich. The synthesis and characterization of 1,4,8,11-tetraazacyclotetradecane ([14]aneN$_4$ or cyclam), 5,12-*rac*-5,7,7,12,14,14-hexamethyl-1,4,8,11-tetraazacyclotetradecane (Me$_6$-[14]aneN$_4$ or tetb), 1,4,8,12-tetraazacyclopentadecane ([15]aneN$_4$), and *meso*-2,12-dimethyl-3,7,11,14-tetraazabicyclo[11.3.1]heptadeca-1(17),13,15-triene (pyo[14]eneN$_4$ or CRH) have been described previously.[47−54] Literature syntheses were used for the [Ru(bpy)-Cl$_4$], [Ru(DMSO)$_4$Cl$_2$], [Ru(NH$_3$)$_4$bpy](PF$_6$)$_2$, [Ru(en)$_2$bpy](PF$_6$)$_2$, and [Ru(py)$_4$bpy](PF$_6$)$_2$ complexes.[28,55−57] Figure 3 contains the skeletal structures of the ligands used in this study.

[Ru([14]aneN$_4$)bpy](PF$_6$)$_2$. The synthesis of this complex has been reported previously.[58,59] That synthesis was modified in this work, as described here, and the modified procedure was used to synthesize most of the macrocyclic ligand complexes. All of the work described was performed in an Ar atmosphere. A 100-mg sample of [Ru(bpy)Cl$_4$] was refluxed with 5 mL of dimethyl sulfoxide (DMSO) in a round-bottomed flask for approximately 20 min. The solution color changed from deep green to light brown. The flask and its contents were cooled to room temperature, then 20 mL of ether was slowly added to the reaction flask, the mixture was swirled for 1 min, and the light-yellow supernatant solution was decanted. This was repeated several times until all of the DMSO solvent was extracted and a brown solid of $Ru^{II}bpy(DMSO)_x$ ($x = 1-4$) adhered to the sides of the flask. A 100-mg quantity of the [14]aneN$_4$ ligand and 10 mL of 1-propanol were added to the Ru solid and refluxed for about 24 h; during this time, the solution color changed from brown to violet. The violet solution was filtered and mixed with 10 mL of water containing 5 g of NH$_4$PF$_6$. The

(39) Englman, R.; Jortner, J. *Mol. Phys.* **1970**, *18*, 145.
(40) Freed, K. F.; Jortner, J. *J. Chem. Phys.* **1970**, *52*, 6272.
(41) Bixon, M.; Jortner, J.; Cortes, J.; Heitele, H.; Michel-Beyerle, M. E. *J. Phys. Chem.* **1994**, *98*, 7289.
(42) Newton, M. D. In *Electron-Transfer in Chemistry*; Balzani, V., Ed.; Wiley-VCH: Weinheim, Germany, 2001; Vol. 1; p 3.
(43) Kober, E. M.; Marshall, J. M.; Dressick, W. J.; Sullivan, B. P.; Caspar, J. V.; Meyer, T. J. *Inorg. Chem.* **1985**, *24*, 2755.
(44) Kober, E. M.; Casper, J. V.; Lumpkin, R. S.; Meyer, T. J. *J. Phys. Chem.* **1986**, *90*, 3722.
(45) Casper, J. V.; Kober, E. M.; Sullivan, B. P.; Meyer, T. J. *J. Am. Chem. Soc.* **1982**, *104*, 630.
(46) Kober, E. M.; Meyer, T. J. *Inorg. Chem.* **1985**, *24*, 106.
(47) Hay, R. W.; Lawrence, G. A.; Curtis, N. F. *J. Chem. Soc., Perkin Trans.* **1975**, 591.
(48) Barefied, E. K.; Wagner, F.; Herlinger, A. W.; Dahl, A. R. *Inorg. Synth.* **1976**, *16*, 221.
(49) Habib, H. S.; Hunt, J. P. *J. Am. Chem. Soc.* **1966**, *88*, 1668.
(50) Hung, Y. *Inorg. Synth.* **1980**, *20*, 108.
(51) Barefied, E. K.; Wagner, F. *Inorg. Synth.* **1976**, *16*, 220.
(52) Barefied, E. K.; Freeman, G. *Inorg. Synth.* **1980**, *20*, 108.
(53) Herve, G.; Bernard, B.; Le Bris, N.; Yaouanc, J.-J.; Handel, H.; Toupet, L. *Tetrahedron Lett.* **1998**, *39*, 6861.
(54) Karn, J. L.; Busch, D. H. *Inorg. Chem.* **1969**, *8*, 1149.
(55) Krause, R. A. *Inorg. Chim. Acta* **1977**, *22*, 209.
(56) Evans, I. P.; Spencer, A.; Wilkinson, G. *J. Chem. Soc., Dalton Trans.* **1973**, 204.
(57) Curtis, J. C.; Sullivan, B. P.; Meyer, T. J. *Inorg. Chem.* **1983**, *22*, 224.
(58) Che, C.-M.; Kwong, S.-S.; Poon, C. K.; Lai, T.-F.; Mak, T. C. W. *Inorg. Chem.* **1985**, *24*, 1359.
(59) Sakai, K.; Yamada, Y.; Tsubomura, T. *Inorg. Chem.* **1996**, *35*, 3163.

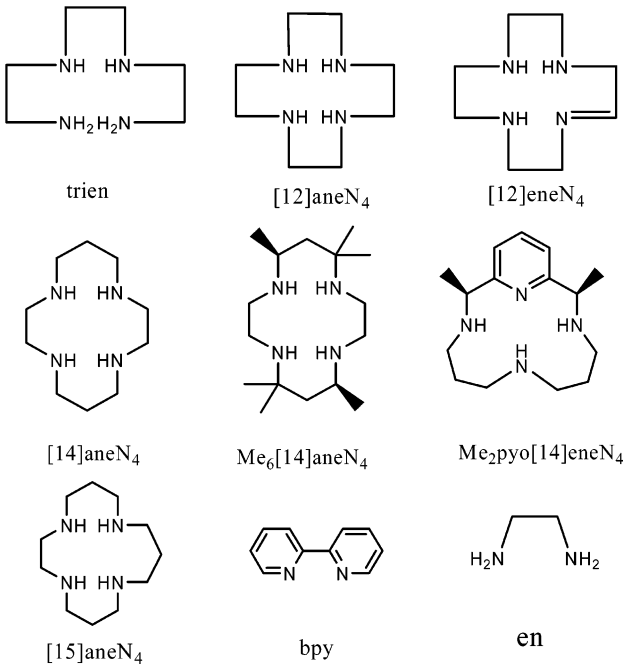

Figure 3. Skeletal structures of some of the ligands and abbreviations used in this study.

volume of the solution was reduced to 10 mL and filtered to obtain the violet product. An acetonitrile solution of this product was passed over an acidic alumina column and eluted with a 1:2 mixture of acetonitrile and toluene. The last third of the violet band was collected, and the solvent was removed by rotary evaporation. The typical yield was 30%. The final product was dissolved in 5 mL of acetone and then combined with 5 mL of acetone half-saturated in NH_4PF_6(aq). This mixture was kept at ice temperature for about 4 days to obtain the product as fine-quality crystals. ^{13}C NMR (acetone-d_6): δ 160.6, 154.9, 135.3, 125.8, 123.6, 54.4, 50.9, 48.5, 47.6, 23.9.

[Ru(trien)bpy](PF$_6$)$_2$, [Ru(pyo[14]eneN$_4$)bpy](PF$_6$)$_2$, and [Ru([15]aneN$_4$)bpy](PF$_6$)$_2$. These complexes were prepared using the procedure for [Ru([14]aneN$_4$)bpy](PF$_6$)$_2$. Yields were typically about 30%. ^{13}C NMR (acetone-d_6): for [Ru(trien)bpy](PF$_6$)$_2$, δ 161.3, 155.1, 135.4, 126.6, 123.7, 56.5, 54.7, 44.1; for [Ru(pyo-[14]eneN$_4$)bpy](PF$_6$)$_2$, δ 166.9, 162.4, 159.4, 154.8, 151.5, 136.7, 136.4, 136.0, 127.5, 126.8, 124.5, 124.0, 121.7, 67.3, 55.5, 52.5, 25.7, 22.3; for [Ru([15]aneN$_4$)bpy](PF$_6$)$_2$, δ 162.1, 161.6, 157.1, 156.5, 136.7, 135.9, 127.0, 126.8, 124.4, 124.2, 56.2, 55.3, 55.1, 55.0, 54.3, 51.8, 50.0, 48.1, 29.2, 28.2, 23.9.

[Ru([12]aneN$_4$)bpy](PF$_6$)$_2$ and [Ru([12]eneN$_4$)bpy](PF$_6$)$_2$. The procedure described for [Ru([14]aneN$_4$)bpy](PF$_6$)$_2$ was also followed for [Ru([12]aneN$_4$)bpy]$^{2+}$, but this procedure resulted in a mixture of [Ru([12]aneN$_4$)bpy]$^{2+}$ and [Ru([12]eneN$_4$)bpy]$^{2+}$. The reaction products were passed over an acidic alumina column and eluted with a 1:1 mixture of CH_3CN and toluene. The recrystallization step resulted in a mixture of the crystals of [Ru([12]aneN$_4$)-bpy](PF$_6$)$_2$ (violet thin plates) and [Ru([12]eneN$_4$)bpy](PF$_6$)$_2$ (light-red needles) in the ratio of about 95:5. We attempted to separate these products by recrystallization at room temperature, but when the recrystallization was repeated three times, the final product was the light-red needles of [Ru([12]eneN$_4$)bpy](PF$_6$)$_2$. We obtained the pure [Ru([12]aneN$_4$)bpy](PF$_6$)$_2$ complex from the initial product mixture by selecting the crystals by hand under a microscope. ^{13}C NMR (acetone-d_6): for [Ru([12]aneN$_4$)bpy](PF$_6$)$_2$, δ 160.7, 150.8, 134.0, 126.0, 124.4, 59.6, 52.6; for [Ru([12]eneN$_4$)bpy](PF$_6$)$_2$, δ 171.4, 159.7, 158.9, 151.4, 151.2, 135.2, 134.7, 126.5, 126.2, 123.9, 123.8, 64.7, 61.0, 59.2, 57.2, 55.4, 53.4, 44.4.

[Ru(Me$_6$[14]aneN$_4$)bpy](PF$_6$)$_2$. A sample of 100 mg of [Ru-(DMSO)$_4$Cl$_2$] dissolved in 20 mL of 1-propanol was refluxed with 150 mg of the ligand for about 4 h. After the golden-yellow solution was cooled to room temperature, 60 mg of bpy was added, and the solution was refluxed for about 2 days. The solution color changed from golden yellow to violet. The product was purified as described for [Ru([14]aneN$_4$)bpy](PF$_6$)$_2$. ^{13}C NMR (acetone-d_6): δ 160.4, 155.1, 135.5, 127.6, 124.2, 58.4, 53.4, 51.7, 48.4, 44.8, 28.6, 26.9, 20.9.

The elemental analyses were performed by Midwest Microlab, LLC (Indianapolis, IN); they are summarized in Table 1.

2. Instrumentation. Details of our procedures and instrumentation can be found elsewhere.[28,32] Emission spectra in 77 K glasses were obtained using a calibrated [Xe emission lines for wavelength and an Oriel model 63358 quartz−tungsten−halogen (QTH) lamp for intensity] Princeton Instruments (Roper Scientific) OMA V InGaAs array detector (512 pixels) mounted on an Acton SP500 spectrometer. A 300-g/mm grating, blazed at 1000 nm, provided an effective observation window of 150 nm, and the WinSpec program was operated in the scan−accumulate−paste mode. Continuous-wave, 532-nm excitation was provided by MGL-S−B 50-mW diode laser modules (Changchun Industries Optoelectronics Tech Co. Ltd., Changchun, China) purchased from OnPoint Lasers, Inc. (Minneapolis, MN). The WinSpec ASCII files were transferred to EXCEL, and up to 50 spectra were averaged for each complex. Luminescence decay rate constants were determined by passing the emitted light through an ISA H-100 monochromator to a Hammamatsu 950 photomultiplier tube coupled to a LeCroy 9310 digital oscilloscope and interfaced to a computer. The decay curves were fitted with single exponentials using the OLIS program as described previously.[60]

The electrochemical measurements were performed with a BAS model 100A electrochemical workstation. Cyclic voltammograms (CVs) were obtained using a three-electrode system consisting of a Ag/AgCl reference electrode, a Pt wire counter electrode, and a Pt disk working electrode for measurements in dry CH_3CN. The solutions consisted of the complex dissolved in acetonitrile containing 0.1 mol/L tetrabutylammonium hexafluorophosphate as the electrolyte; good quality CVs of Ru complexes with macrocyclic ligands were generally only obtained in weakly acidic ($\sim 10^{-3}$ M) solutions. Ferrocene was dissolved in the sample solutions as an internal reference (0.437 V vs Ag/AgCl) for the CVs.

UV−visible spectra were recorded using a Shimadzu UV-2101PC spectrophotometer. The ^{1}H and ^{13}C NMR spectra were performed using a Varian 300-Hz instrument.

3. X-ray Structure Determinations. Diffraction data were measured on a Bruker X8 APEX-II κ geometry diffractometer[61] with Mo radiation and a graphite monochromator at 100 K. Frames were collected as a series of sweeps with the detector at 40 mm and 0.3° between each frame. Frames were recorded for 10−20 s. The structures were solved and refined with Sheldrick's *SHELX-97*.[62] A summary of the crystallographic parameters is given in Table 2, and further details can be found in the Supporting Information.[63]

(60) Song, X.; Lei, Y.; Van Wallendel, S.; Perkovic, M. W.; Jackman, D. C.; Endicott, J. F.; Rillema, D. P. *J. Phys. Chem.* **1993**, *97*, 3225.
(61) *APEX II, collection and processing programs are distributed by the manufacturer*; Bruker AXS Inc.: Madison, WI, 2004.
(62) Sheldrick, G. *SHELX-97*; University of Gottingen: Gottingen, Germany, 1997.
(63) Supporting Information: see paragraph at the end of this paper.

Table 1. Elemental Analysis for $[Ru(Am)_4bpy]^{2+}$ Complexes

$(Am)_4$ ligand	formula	anal. calcd: C %, H %, N %	anal. found: C %, H %, N %
$Me_2pyo[14]aneN_4$	$C_{28}H_{40}N_6Ru_1P_2F_{12}$	38.76, 4.65, 9.69	38.41, 4.59, 9.62
$Me_6[14]aneN_4$	$C_{26}H_{44}N_6Ru_1P_2F_{12}$	37.55, 5.33, 10.10	37.35, 5.31, 9.81
$[14]aneN_4$	$C_{20}H_{32}N_6Ru_1P_2F_{12}$	32.14, 4.31, 11.24	32.18, 4.40, 10.98
$[15]aneN_4$	$C_{21}H_{34}N_6Ru_1P_2F_{12}$	33.12, 4.50, 11.04	32.96, 4.57, 10.94
$[12]eneN_4$	$C_{18}H_{26}N_6Ru_1P_2F_{12}$	30.13, 3.65, 11.71	29.80, 3.53, 11.38
$[12]aneN_4$	$C_{18}H_{28}N_6Ru_1P_2F_{12}$	30.05, 3.92, 11.68	29.39, 3.84, 11.18
trien	$C_{16}H_{26}N_6Ru_1P_2F_{12}$	27.71, 3.37, 12.12	27.76, 3.37, 12.00

Table 2. Crystal Data for $[Ru(bpy)L]^{2+}$ Complexes

	$[Ru(trien)bpy](PF_6)_2$	$[Ru([12]aneN_4)bpy](PF_6)_2$	$[Ru(NH_3)_4bpy](PF_6)_2 \cdot 0.5CH_3OH \cdot 0.5H_2O$	$[Ru(Me_6[14]aneN_4)bpy](PF_6)_2 \cdot H_2O$
formula	$C_{16}H_{26}F_{12}N_6P_2Ru$	$C_{18}H_{28}F_{12}N_6P_2Ru$	$C_{10.5}H_{23}F_{12}N_6O_1P_2Ru$	$C_{26}H_{46}F_{12}N_6OP_2Ru$
fw	693.44	719.47	640.36	849.70
space group	*P*2(1)/*c*	*P*2(1)/*c*	*P*2/*c*	*P*2(1)2(1)2(1)
a (Å)	11.3329(4)	11.3860(3)	11.2905(2)	9.6939(2)
b (Å)	14.7900(4)	15.3588(4)	17.7414(4)	10.2598(3)
c (Å)	14.3292(4)	14.3446(4)	10.8096(2)	34.0818(9)
β (deg)	90.824(1)	90.573(1)	93.294(3)	
V (Å^3)	2401.5(1)	2508.4(1)	2161.69(7)	3389.69(15)
Z	4	4	4	4
temp (K)	100(2)	100(2)	100(2)	100(2)
λ (Å)	0.71073	0.71073	0.71073	0.71073
d_{calcd} (g cm^{-3})	1.918	1.905	1.968	1.665
μ (mm^{-1})	0.899	0.864	0.992	0.656
$R(F)$ (%)[a]	4.05	3.50	4.30	3.39
$R_w(F)$ (%)[a]	8.75	8.20	12.37	6.41

[a] $R(F) = \sum|F_o| - |F_c|/\sum|F_o|$; $R_w(F) = [\sum w(F_o^2 - F_c^2)^2/\sum w(F_o^2)^2]^{1/2}$ for $I > 2\sigma(I)$.

Crystals of $[Ru(trien)bpy][PF_6]_2$ appeared as dark plates, and a sample of approximately 0.16 × 0.14 × 0.06 mm^3 was used for data collection. A total of 2943 frames were collected, yielding 44 210 reflections, of which 7800 were independent. H positions were placed in observed positions and refined. The asymmetric unit contains one cation and two anions without solvent.

$[Ru([12]aneN_4)bpy][PF_6]_2$ crystallized as red rods. The sample used for data collection was approximately 0.3 × 0.08 × 0.08 mm^3. A total of 3048 frames were collected, yielding 39 585 reflections, of which 7902 were independent. H positions were placed in observed positions and refined. The asymmetric unit contains one cation and two anions without solvent.

A dark-amber plate of $[Ru(NH_3)_4bpy][PF_6]_2 \cdot 0.5[CH_3OH] \cdot 0.5H_2O$ sized 0.22 × 0.12 × 0.04 mm^3 was used for data collection. A total of 2954 frames were recorded, yielding 62 307 reflections, of which 6818 were independent. We were unable to obtain an untwinned sample, so a crystal with approximately 30% twinning represented by a 180° rotation about the *c* axis was used, and refinement on two simultaneous matrixes ensued. One set of F atoms in PF_6 showed typical disorder and was kept isotropic. Likewise, the C atom of the $^1/_2$ equiv of methanol was kept isotropic. No H atoms were placed on the solvates in the model because of disorder. Other H positions were calculated. The asymmetric unit contains one cation, two anions, and $^1/_2$ equiv each of methanol and water.

A dark rod of approximately 0.16 × 0.08 × 0.06 mm^3 of $[Ru(Me_6[14]aneN_4)bpy](PF_6)_2 \cdot H_2O$ was used for data collection. A total of 2135 frames were integrated, which yielded 28 751 reflections, of which 8350 were unique. H atoms were placed in observed and calculated positions. Racemic twinning refined to 50%. The asymmetric unit contains one cation, two anions, and 1 equiv of solvent water.

4. Data Analysis Procedures. The procedures that we used are described in detail elsewhere,[28,32] and only particularly pertinent features are summarized here.

The Gaussian components that represent the emission fundamentals, $I_{\nu_{m(f)}}$, were obtained by adjusting the intensity of the emission maximum to 1.00 in the spectral Excel files and then transferring the files to Grams32 in order to obtain $h\nu_{max(f)}$ and $\Delta\nu_{1/2}$ from the Gaussian deconvolution of the spectrum. The emission intensity at a frequency ν_m can be represented as[23,64−66]

$$I_{\nu_m} = \frac{64\pi^4}{3h^3c^3 \ln 10} \frac{\nu_m \eta^3 H_{eg}{}^2 (\Delta\mu_{eg})^2}{(4\pi\lambda_s k_B T)^{1/2}} \mathrm{FC} \quad (5)$$

where η is the index of refraction, ν_m is the frequency of the incident radiation, $(H_{eg}/h\nu_{eg})\Delta\mu_{eg}$ has been substituted for the transition dipole, M_{eg},[23,66,67] H_{eg} is the electronic matrix element, $\Delta\mu_{eg}$ is the difference of excited- and ground-state dipole moments, λ_s is the reorganizational energy of the solvent and other displacement modes with frequencies $\nu_s < 4k_BT$, and *c* is the speed of light. On the basis of Gaussian band shapes and a wave packet model and for the contributions of a single vibrational mode, FC can be represented by[23,64,65]

$$\mathrm{FC} = \sum\nolimits_j F_{j,k}[e^{-(4G_j^2 \ln 2/\Delta\nu_{1/2}^2)}] \quad (6)$$

$$F_{j,k} = \frac{S_k^j e^{-S_k}}{j!}$$

$$S_k = \lambda_k/h\nu_k \quad (7)$$

$$G_j = E_{ge}{}^{0\prime 0} - \lambda_s - jh\nu_k - h\nu_m \quad (8)$$

It is convenient to use $h\nu_{max(f)} = E_{ge}{}^{0\prime 0} - \lambda_s$ because $E_{ge}{}^{0\prime 0}$ and λ_s are difficult to determine independently, and the intensity of the

(64) Myers, A. B. *Chem. Rev.* **1996**, *96*, 911.
(65) Myers, A. B. *Acc. Chem. Res.* **1998**, *30*, 5519.

fundamental at a frequency ν_m is

$$I_{\nu_m}(f) \cong I_{\max(f)} e^{-\{[h\nu_{\max(f)} - h\nu_m]^2/(\Delta\nu_{1/2}{}^2/4 \ln 2)\}} \quad (9)$$

5. Evaluation of the Vibronic Contributions to the Emission Spectra in a Frozen Solution. The vibronic contributions to the emission spectra can be organized into the respective sums of first-order, $I_{\nu_m(0'1)}$, second-order, $I_{\nu_m(0'2)}$, third-order, $I_{\nu_m(0'3)}$, etc., Gaussian contributions.[27,28] The intensity at a frequency ν_m can be represented as the sum of these components[28]

$$I_{\nu_m} \cong I_{\nu_m(f)} + I_{\nu_m(0'1)} + I_{\nu_m(0'2)} + I_{\nu_m(0'3)} + ... \quad (10)$$

The difference spectrum is constructed from the observed emission spectrum, $I_{\nu_m(expt)}$, as $I_{\nu_m(diff)} = I_{\nu_m(expt)} - I_{\nu_m(f)}$, where the contributions of the fundamental component are determined from a Grams32 fit of the observed spectrum.[28]

When the distortions, a_k, are small in the coordinates, Q_k, that correlate the differences in excited- and ground-state geometries (i.e., $\lambda_k/h\nu_k \leq 0.1$, where $\lambda_k = (1/2)f_k(a_k)^2$ is the vibrational reorganizational energy and ν_k is the frequency for the kth vibrational mode), then the intensity of the kth first-order vibronic contribution to the emission spectrum is given by eq 1.[35,36] The empirical reorganizational energy profiles (emreps) are based on eq 2, and they are generated by multiplying the difference spectrum by the difference between $h\nu_{\max(f)}$ and the observed emission energy $[h\nu_d = h(\nu_{\max(f)} - \nu_m)]$. This procedure generates an envelope of the convoluted contributions of the reorganizational energies; thus, with $w = \Delta\nu_{1/2}/4 \ln 2$, the first-, second-, and third-order contributions, respectively, are given by

$$\xi_i = h\nu_d \sum_i \left[\left(\frac{\lambda_i}{h\nu_i} \right) e^{-(G_i/w)^2} \right]$$

$$G_i = h\nu_{\max(f)} - h\nu_i \quad (11)$$

$$\xi_{ij} = h\nu_d \frac{1}{2} \sum_i \sum_j \left[\left(\frac{\lambda_i}{h\nu_i} \right) \left(\frac{\lambda_j}{h\nu_j} \right) e^{-(G_{ij}/w)^2} \right]$$

$$G_{ij} = h\nu_{\max(f)} - h\nu_i - h\nu_j \quad (12)$$

$$\xi_{ijk} = h\nu_d \frac{1}{6} \sum_i \sum_j \sum_k \left[\left(\frac{\lambda_i}{h\nu_i} \right) \left(\frac{\lambda_j}{h\nu_j} \right) \left(\frac{\lambda_k}{h\nu_k} \right) e^{-(G_{ijk}/w)^2} \right]$$

$$G_{ijk} = h\nu_{\max(f)} - h\nu_i - h\nu_j - h\nu_j \quad (13)$$

However, because $h\nu_d$ is a variable, the functions described by eqs 11−13 are not Gaussian, and in order for the maximum amplitudes of the individual reorganizational energy components to occur at the frequencies of the distortion modes, a correction must be made. A relatively simple correction is based on the first-order vibronic terms;[28] thus, we set $h\nu_x = 2(h\nu_d) - [(h\nu_d)^2 + (\Delta\nu_{1/2})^2/4 \ln 2]^{1/2}$ and $\rho_i = \xi_i(\nu_x/\nu_d)$, etc., so that

$$\Lambda_x = \sum_i [\rho_i + \sum_j (\rho_{ij} + \sum_k \rho_{ijk})] \quad (14)$$

Thus, the emrep is obtained from the experimental spectrum by (a) determining a fundamental component by means of a careful fit of the observed spectrum using Grams 32, (b) subtracting the fundamental component from the observed spectrum (using data files in EXCEL) to obtain the difference spectrum, (c) constructing Λ_x based on eq 14, and then (d) plotting Λ_x vs $h\nu_x$.[27,28,32] In principle,

$$\Lambda_x = h\nu_x \left[\frac{I_{\nu_m(diff)}}{I_{\max(f)}} \right] = \frac{h\nu_x}{I_{\max(f)}} [I_{\nu_m(0'1)} + I_{\nu_m(0'2)} + I_{\nu_m(0'3)} + ...] \quad (15)$$

As a consequence of the component bandwidths and overlapping first-, second-, third-order, etc., contributions in eqs 10−15, our procedure provides information about the differences in reorganizational energy amplitudes for a closely related series of complexes; however, when there are a large number of vibrational modes whose energy differences (Δh_k) are smaller than the component bandwidths ($\Delta\nu_{1/2}$), the emrep amplitudes will be much larger than any individual vibrational reorganizational energy, and if only first-order terms contribute in the frequency range of interest, then the emrep amplitude is less than the sum of all of the first-order vibrational reorganizational energies. However, in the systems considered here, there will also be contributions to emrep amplitudes from the overlap with higher-order terms; the overlap with the higher-order terms will contribute approximately the same percentage to the emrep and the emission spectrum amplitudes. We have previously used the rR parameters for $[Ru(bpy)_3]^{2+}$ and $[Ru(NH_3)_4bpy]^{2+}$ to examine the implications and uncertainties of this procedure.[28] It is important to note that the procedures outlined here and presented in more detail elsewhere[28] are dependent on obtaining a good estimate of the fundamental and that the deconvolutions of the fundamental have been shown to be reliable when the fundamental is the dominant component of the spectrum (i.e., all $S_i \ll 1$) and for bandwidths less than about 1200 cm^{-1}.[28] The 77 K emission spectra of $[Ru(L)_4bpy]^{2+}$ complexes satisfy these conditions. In general, the rR modeling indicates that the Grams32 fitting procedure does overestimate the intensity of the fundamental component by 10−30% when $\Delta\nu_{1/2} \approx 1000$ cm^{-1} and the discrepancy increases with the bandwidth; however, the estimates of $h\nu_{\max(f)}$ and $\Delta\nu_{1/2}$ deviate from the correct values by much less than 10%.[28] Within a series of related complexes, the corrections of $\Lambda_{x(max)}$ for differences in the bandwidth are relatively small, and these are described below.

6. Corrections. Because the bandwidths found for the charge-transfer emissions in 77 K frozen solutions are large ($\Delta\nu_{1/2} = 600-1100$ cm^{-1}), the fundamentals obtained in the Grams32 deconvolutions contain contributions from vibrational modes with $h\nu_{\max(f)} - h\nu_h < \sim\Delta\nu_{1/2}$, and this results in intensity amplitudes that are too large by 10−30%.[28] The errors in this and other parameters obtained from the emission spectra by our procedures can be represented as functions of the intrinsic bandwidth, $\Delta\nu_{1/2}$.[28] We use corrections based on the rR parameters for the $[Ru(NH_3)_4bpy]^{2+}$ [31] and $[Ru(bpy)_3]^{2+}$ [30] complexes in assessing the variations in the spectroscopic parameters for the $[Ru(L)_4bpy]^{2+}$ complexes;[28] these two complexes bracket the range of bandwidths for these complexes. The bandwidth corrections for $[Ru(bpy)_3]^{2+}$ are given by[28]

$$\Lambda_{x(corr)} = \Lambda_{x(max)}[1 - (3.27 \pm 0.09)|\partial\Delta\nu_{1/2}| \times 10^{-4}] \quad (16)$$

and for $[Ru(NH_3)_4bpy]^{2+}$

$$\Lambda_{x(corr)} = \Lambda_{x(max)}[1 - (4.89 \pm 0.17)|\partial\Delta\nu_{1/2}| \times 10^{-4}] \quad (17)$$

(66) Myers, A. B. In *Laser Techniques in Chemistry*; Myers, A. B., Rizzo, T. R., Eds.; John Wiley & Sons: New York, 1995; Vol. XXIII; p 325.
(67) Yardley, J. T. *Introduction to Molecular Energy Transfer*; Academic: New York, 1980.

The first-order components, $\Lambda_{x(0'1)}$, contribute only 89% and 71%, respectively, for these complexes to the total emrep intensities near $h\nu_{x(\max)} \approx 1500$ cm^{-1}, with the remaining contributions to the amplitude arising mostly from overlapping second-order terms, $\Lambda_{x(0'2)}$.[28] The vibrational reorganizational energies, λ_k, inferred from the rR spectra are small (397[30] and 224[31] cm^{-1}, respectively for $\nu_k \approx 1490$ cm^{-1}), and more than half of the amplitudes of the maxima of the corresponding first-order emreps, $\Lambda_{x(\max)}$, are a consequence of the finite bandwidths of the components and the significant number of vibronic components with energies of about $1490 \pm \Delta\nu_{1/2}$ cm^{-1}. We have corrected $\Lambda_{x(\max)}$ for bandwidth variations within the series of complexes based on eqs 16 and 17. The variations of $\Lambda_{x(\max)}$ have been shown to be reasonable estimates of the variations in the amplitudes of λ_k.[28]

Results

1. Syntheses. While syntheses of $[Ru(Am)_4bpy]^{2+}$ complexes using the literature procedures[58,59] worked for most complexes, we did not find them useful for $(Am)_4 = Me_6[14]aneN_4$. For this complex, syntheses that combined the $[Ru(DMSO)_4Cl_2]$[56] starting material with the macrocyclic ligand were more successful. We found the $[Ru([12]aneN_4)bpy]^{2+}$ complex to be the most difficult to handle of the complexes employed in this study. In our hands, the $[Ru([12]aneN_4)bpy]^{2+}$ complex oxidized to the $[Ru([12]eneN_4)bpy]^{2+}$ complex in all of our attempts to purify the complex by recrystallization in neutral solutions or upon any exposure to air under ambient conditions. For example, our electrochemical studies of $[Ru([12]aneN_4)bpy]^{2+}$ were complicated by its oxidation in the course of successive scans, most likely by the diffusion of dioxygen into the Ar-purged sample in the electrochemical cell; the differential pulse voltammograms that illustrate the oxidation of the $[12]aneN_4$ complex are shown in Figure S1 in the Supporting Information.[63] This sensitivity to oxidation in neutral solutions and the isolation of a single conformational isomer[68] contrast to the properties recently reported for this complex.[69] The $[Ru([12]eneN_4)bpy]^{2+}$ complex has a distinctive ^{13}C NMR peak at 171 ppm that is assigned to the imine moiety of the macrocyclic ligand. The ^{1}H and ^{13}C NMR spectra indicated that our syntheses yielded only a single conformational isomer of the $[Ru([12]aneN_4)bpy]^{2+}$ complex. The ^{13}C NMR spectra provide an especially useful structural probe for this group of complexes because ^{13}C NMR spectra of all of the complexes with a C_2 symmetry axis bisecting the bpy ligand have only 5 aromatic C peaks, while the spectra of those complexes without such a C_2 axis have 10 aromatic C peaks. The $[Ru([12]aneN_4)bpy]^{2+}$ complex is a particularly nice example because its spectrum contains only five aromatic and two aliphatic C peaks, consistent with its C_{2v} symmetry and in clear contrast to the $[Ru([12]eneN_4)bpy]^{2+}$ complex, which has 10 aromatic, 1 imine, and 7 aliphatic C peaks as expected for C_1 symmetry. Similarly, the ^{13}C NMR spectrum of $[Ru(pyo[14]eneN_4)bpy]^{2+}$ indicates appreciable asymmetry, and this is most consistent with a structure in which the N(pyridyl) atom of the macrocyclic ring is in the plane of the bpy ligand, as shown in Figure S2 in the Supporting Information.[63]

2. X-ray Crystal Structures. The crystal structure of $[Ru([12]aneN_4)bpy](PF_6)_2$ is the syn,syn structural isomer[46] with all four amine protons on the bpy side of the macrocyclic ligand, similar to the structure reported for $[Zn([12]aneN_4)bpy](ClO_4)_2$.[70] The anti,anti form of the complex $[Ru(Me_6[14]aneN_4)bpy](PF_6)_2$, with the amine protons on alternate sides on the macrocyclic ligand, is similar to the structure reported for $[Ru([14]aneN_4)bpy](BF_4)_2$.[59] Selected bond distances and angles of $[Ru(NH_3)_4bpy]^{2+}$, $[Ru(trien)bpy]^{2+}$, $[Ru([12]aneN_4)bpy]^{2+}$, $[Ru([14]aneN_4)bpy]^{2+}$, and $[Ru(Me_6[14]aneN_4)bpy]^{2+}$ are compared in Table 3; the atom-numbering scheme used is shown in Figure 4. The effects of the different ligands on the stereochemistry of the coordinated bpy ligand are compared in Figure 5. Repulsions between the *gem*-methyl moieties of $Me_6[14]aneN_4$ and bpy result in the largest deformations, while the bpy ligand is only slightly perturbed by the trien and $[12]aneN_4$ ligands and it is very close to the expected planar structure in $[Ru(NH_3)_4bpy]^{2+}$. Thus, the bpy ligand of $[Ru([12]aneN_4)bpy]^{2+}$ is slightly tilted with respect to the $Ru-(Am)_4$ axes by 6−7° (the difference between the N(2)−Ru−N(1) and N(2)−Ru−N(1′) angles in Table 3), and this is readily attributed to the stereochemical repulsions of the N(3) and N(3′) equatorial amine H atoms. The tilt is larger (18−20°), and the bpy ligand is significantly twisted from the usual planar conformation (by 18°) in $[Ru(Me_6[14]aneN_4)bpy]^{2+}$.

3. Electrochemistry. The electrochemical oxidations and reductions of the complexes are summarized in Table 4. The corresponding half-wave potentials are assigned to the Ru^{III}/Ru^{II} and bpy^0/bpy^- couples, respectively. The $E_{1/2}(bpy^{0,-1})$ potential of $[Ru(py)_4bpy]^{2+}$ is about 0.2−0.3 V more positive than those of the other mono(bipyridine)ruthenium complexes. The $Ru^{3+,2+}$ potentials of most of the mono(bipyridine)ruthenium complexes span the range of 0.6−0.9 V, while that of $[Ru(py)_4bpy]^{2+}$ is 1.38 V.

4. Absorption and Emission Spectra. The pertinent absorption and emission spectra, the fundamentals deconvoluted from the ambient absorption spectra (in butyronitrile), and the lifetime data are summarized in Table 5. Because the ambient spectral bandwidths of the complexes are very large (∼2000−3000 cm^{-1}) and because the observed absorption spectra are broad and unstructured, there is considerable uncertainty in their Grams32 fittings. While our spectral modeling based on rR parameters suggests that our procedure intrinsically underestimates $E^{0'0}$ and overestimates $\Delta\nu_{1/2}$ by 2−3% for the ambient bandwidths,[28] this is most likely a lower limit on the experimental uncertainties, which also include contributions of spectral resolution, sample-to-sample reproducibility (probable uncertainties of ≤1% each; we did not average absorption spectra), and the likely convolution of transitions to different electronic states; as a consequence,

(68) We obtain a half-wave potential that is 200 mV smaller than that reported by Ferreira et al.,[69] probably as a consequence of a difference in the reference potentials (E. Tfouni, private communication, 2006). The reported MLCT absorption maximum is similar to ours; it is difficult to compare the ^{1}H NMR spectra.

(69) Ferreira, K. Q.; Cardoso, L. N.; Nikolaou, S.; da Rocha, Z. N.; da Silva, R. S.; Tfouni, E. *Inorg. Chem.* **2005**, *44*, 5544.

(70) Lu, T.-H.; Panneerselvam, K.; Chen, L.-H.; Lin, Y. J.; Liao, F.-L.; Chung, C.-S. *Anal. Sci.* **2001**, *17*, 571.

Table 3. Comparison of Bond Lengths and Angles Determined in X-ray Structures of $[Ru(Am)_4bpy]^{2+}$ Complexes

	$(L)_4$ =				
structural feature	$(NH_3)_4$	trien	$[12]aneN_4$	$[14]aneN_4$[a]	$Me_6[14]aneN_4$
Ru−N(2), Ru−N(2′) [am(m)ine]	2.147, 2.133	2.136, 2.121	2.130, 2.117	2.065, 2.083	2.160, 2.152
Ru−N(3), Ru−N(3′)	2.159, 2.156	2.124, 2.145	2.103, 2.103	2.107, 2.121	2.136, 2.140
Ru−N(1), Ru−N(1′) [bpy]	2.039, 2.046	2.032, 2.047	2.078, 2.080	2.065, 2.083	2.103, 2.092
N(1)−C(1), N(1′)−C(1′)	1.364, 1.358	1.312, 1.370	1.359, 1.364	1.335, 1.350	1.365, 1.354
N(1)−C(5), N(1′)−C(5′)	1.346, 1.350	1.350, 1.351	1.360, 1.354	1.378, 1.368	1.351, 1.367
C(1)−C(1′)	1.475	1.466	1.468	1.473	1.458
C(1)−C(2), C(1′)−C(2′)	1.385, 1.393	1.394, 1.392	1.391, 1.390	1.368, 1.466	1.385, 1.399
C(2)−C(3), C(2)−C(3′)	1.375, 1.369	1.382, 1.385	1.377, 1.382	1.360, 1.408	1.368, 1.367
C(3)−C(4), C(3′)−C(4′)	1.383, 1.389	1.388, 1.385	1.382, 1.383	1.355, 1.281	1.371, 1.382
C(4)−C(5), C(4′)−C(5′)	1.371, 1.391	1.382, 1.385	1.375, 1.380	1.338, 1.311	1.377, 1.379
N(2)−Ru−N(3), N(2)−Ru−N(3′)	88.83, 90.98	80.66, 94.83	81.80, 82.16	91.19, 81.52	82.70, 86.59
N(2′)−Ru−N(3), N(2′)−Ru−N(3′)	88.25, 88.05	96.17, 81.74	81.83, 82.34	82.54, 90.26	86.34, 82.54
N(3)−Ru−N(3′)	85.14	81.79	96.76	86.94	89.70
N(2)−Ru−N(2′)	176.99	175.67	155.91	169.94	164.59
C(6)−N(2)−C(6′), C(6″)−N(2′)−C(6‴)			113.73, 113.22	111.11, 105.58	111.31, 111.22
C(7)−N(3)−C(7′), C(7″)−N(3′)−C(7‴)			118.99, 117.81	117.68, 115.06	111.99, 111.87
N(2)−Ru−N(1), N(2)−Ru−N(1′)	90.25, 88.51	93.83, 95.14	103.50, 96.94	95.94, 94.48	86.57, 106.34
N(2′)−Ru−N(1), N(2′)−Ru−N(1′)	88.25, 88.05	89.58, 88.04	94.59, 102.06	92.70, 92.35	105.61, 85.83
N(3)−Ru−N(1), N(3′)−Ru−N(1′)	98.75, 97.20	101.23, 99.07	91.90, 92.49	97.65, 97.97	97.33, 96.66
N(1)−Ru−N(1′)	78.97	78.54	79.10	77.97	77.66
N(1)−C(1)−C(1′)−N(1′) torsion	3.93	1.98	3.04	0.35	18.24

[a] From ref 59.

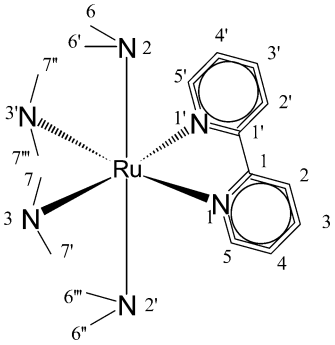

Figure 4. Scheme used for numbering atoms in Table 3.

the overall uncertainties for the estimates of $E^{0\prime 0}$ based on absorption spectra are probably close to 10%. The discussions of absorption energies below employ the observed absorption maxima rather than the deconvoluted absorption fundamentals. In contrast, the uncertainties in energy maxima and bandwidths of the fundamentals deconvoluted from the 77 K emission spectra of the Ru−bpy complexes are probably less than 0.5% because[28,33] (a) the bandwidths are relatively small at 77 K, (b) only two electronic states are involved, (c) most of the intensity of the dominant emission feature arises from the fundamental component, and (d) we have averaged 20−40 separate scans for each emission spectral determination.

The 77 K emission spectra of the $[Ru(Am)_4bpy]^{2+}$ complexes are compared in Figure 6, and Figure 7 compares some of these spectra to those of the $[Ru(L)bpy]^{2+}$ complexes where ligand L contains one or more imine moieties. The vibronic sidebands are much weaker for the $[Ru([12]aneN_4)bpy]^{2+}$ and $[Ru([12]eneN_4)bpy]^{2+}$ complexes than for the other mono(bipyridine)ruthenium complexes with emissions in the same energy range.

5. Emreps. The emreps of the $[Ru(Am)_4bpy]^{2+}$ complexes are compared in Figure 8, and the frequencies and amplitudes of the emrep maxima are recorded in Table 5.

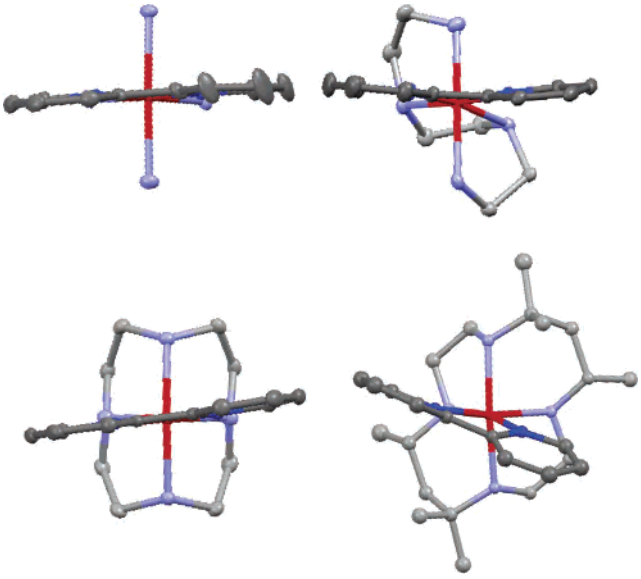

Figure 5. Comparison of the bpy ligand coordination in the X-ray crystal structures of (clockwise from upper left): $[Ru(NH_3)_4bpy](PF_6)_2$; $[Ru(trien)bpy](PF_6)_2$; $[Ru([12]aneN_4)bpy](PF_6)_2$; $[Ru(Me_6\text{-}[14]aneN_4]bpy](PF_6)_2$. Structures are aligned for viewing parallel to the plane of at least one pyridyl moiety of bpy and orthogonal to one ("vertical") coordination axis of Ru. Constructed from X-ray data using Mercury 1.4.

6. Excited-State Rate Constants. The excited-state decays gave excellent fits to single exponentials, with a decay rate constant k_d. The excited-state lifetimes, τ_e, are the inverse of k_d. The observed decay rate constants can be represented by the sum of the radiative, k_r, and nonradiative rate constants for excited-state decay: $k_d = k_r + k_{nr}$. We neglect the k_r contributions in the discussion below, assuming that $k_d \approx k_{nr}$ because the radiative quantum yields are small even for the longest-lived complex, $[Ru(bpy)_3]^{2+}$,[71] and the small corrections for k_r have no relevance in the order of magnitude deviations discussed below. Assuming that k_r is temperature-

(71) Van Houten, J.; Watts, R. J. *J. Am. Chem. Soc.* **1975**, *97*, 3843.

Table 4. Half-Wave Potentials of the Complexes[a]

complexes	$E_{1/2}$, V		$F\Delta E_{1/2}$, eV ($cm^{-1}/10^4$)[b]
	$Ru^{3+/2+}$	$bpy^{0/1-}$	
$[Ru(bpy)_3]^{2+}$ [c]	1.27 ± 0.01	−1.34 ± 0.01	2.61 ± 0.02 (2.10 ± 0.02)
$[Ru(en)(bpy)_2]^{2+}$ [c]	1.00 ± 0.01	−1.42 ± 0.01	2.42 ± 0.02 (1.95 ± 0.02)
$[Ru(NH_3)_2(bpy)_2]^{2+}$ [c]	0.95 ± 0.01	−1.44 ± 0.01	2.39 ± 0.02 (1.93 ± 0.02)
$[Ru(py)_4bpy]^{2+}$	1.38 ± 0.01	−1.32 ± 0.01	2.70 ± 0.02 (2.18 ± 0.02)
$[Ru([12]eneN_4)bpy]^{2+}$	0.84 ± 0.01	−1.58 ± 0.01	2.42 ± 0.02 (1.95 ± 0.02)
$[Ru(pyo[14]eneN_4)(bpy)]^{2+}$	0.88 ± 0.01	−1.52 ± 0.01	2.40 ± 0.02 (1.94 ± 0.02)
$[Ru(Me_6aneN_4)(bpy)]^{2+}$	0.87 ± 0.01	−1.54 ± 0.01	2.41 ± 0.02 (1.94 ± 0.02)
$[Ru([14]aneN_4)bpy]^{2+}$ [d]	0.85 ± 0.01	−1.55 ± 0.01	2.40 ± 0.02 (1.94 ± 0.02)
$[Ru([15]aneN_4)bpy]^{2+}$	0.84 ± 0.01	−1.51 ± 0.01	2.35 ± 0.02 (1.90 ± 0.02)
$[Ru([12]aneN_4)bpy]^{2+}$	0.70 ± 0.01	−1.58 ± 0.01	2.28 ± 0.02 (1.84 ± 0.02)
$[Ru(trien)bpy]^{2+}$	0.68 ± 0.01	−1.59 ± 0.01	2.27 ± 0.02 (1.83 ± 0.02)
$[Ru(en)_2bpy]^{2+}$ [c]	0.68 ± 0.01	−1.62 ± 0.01	2.30 ± 0.02 (1.85 ± 0.02)
$[Ru(NH_3)_4bpy]^{2+}$ [c]	0.61 ± 0.01	−1.64 ± 0.01	2.25 ± 0.02 (1.81 ± 0.02)

[a] Sweep rate, 100 mV/s; electrolyte/solvent, 0.1 M TBAH/CH_3CN; Ag/AgCl reference electrode, $E_{1/2}$ of ferrocene is 0.437 V; F = Faraday's constant. [b] $\Delta E_{1/2} = E_{1/2}(Ru^{3+/2+}) - E_{1/2}(bpy^{0/1-})$. [c] Reference 17. [d] Reference 28.

Table 5. Spectroscopic Properties and Excited-State Decay Rate Constants for $[Ru(Am)_{6-2n}(bpy)_n]^{2+}$ Complexes[a]

Ru^{II} complex	$h\nu_{max(abs)}$ ⟨$\epsilon/10^3$⟩ {$h\nu_{max(f)}$ [$\Delta\nu_{1/2}$]}, 298 K[c]	$h\nu_{max(em)}$, 298 K	$h\nu_{max(em)}$, 77 K	$h\nu_{max(f)}$ [$\Delta\nu_{1/2}$], 77 K {$h\nu_{max(f)}$ [$\Delta\nu_{1/2}$], 298 K}	$\Lambda_x(\nu_x)$, 77 K	k_d (μs^{-1}),[d] 77 K {k_d (μs^{-1}),[d] 298 K}
$[Ru(bpy)_3]^{2+}$ [b]	21.9 (d/w)	15.98 (d/w)	17.12 (d/w)	17.22 [0.68] (d/w)	1.16 (1.49) (d/w)	0.23 (d/w){1.1 (d/w)}
	22.1 (bun) ⟨12.4⟩{22.1 [2.2]}[c]			{16.53 [1.64] (d/w)}		
		16.24 (bun)	17.25 (bun)	17.31 [0.64] (bun)	1.05 (1.50) (bun)	0.13 (bun){4.3 (bun)}
$[Ru(en)(bpy)_2]^{2+}$ [b]	20.2 (d/w)	13.97 (d/w)	15.00 (d/w)	15.06 [0.78] (d/w)	1.00 (1.50) (d/w)	1.3 (d/w){12.3 (d/w)}
	20.4 (bun)	14.35 (bun)	15.11 (bun)	15.16 [0.72] (bun)	0.88 (1.49) (bun)	0.69 (bun){10.2 (bun)}
$[Ru(NH_3)_2(bpy)_2]^{2+}$ [b]	20.4 (d/w)	13.52 (d/w)	14.56 (d/w)	14.64 [0.91] (d/w)	0.99 (1.53) (d/w)	2.9 (d/w){25 (d/w)}
	20.2 (bun)	13.98 (bun)	14.67 (bun)	14.70 [0.78] (bun)	0.86 (1.49) (bun)	1.7 (bun){14.5 (bun)}
$[Ru(py)_4bpy]^{2+}$ [c]	22.6 (bun) ⟨5.9⟩{22.5 [2.4]}		16.87 (bun)	16.91 [0.89] (bun)	0.90 (1.40) (bun)	0.13 (bun)
$[Ru([12]eneN_4)bpy]^{2+}$ [c]	20.1 (bun) ⟨5.3⟩{20.1 [3.1]}		14.49 (bun)	14.56 [0.91] (bun)	0.57 (1.34) (bun)	0.126 (bun)
$[Ru(pyo[14]eneN_4)bpy]^{2+}$ [c]	20.0 (bun) ⟨7.1⟩{20.0 [2.2]}	13.56 (bun)	14.16(bun)	14.22[0.98](bun)	0.91 (1.48) (bun)	1.6 (bun){>80 (bun)}
$[Ru(Me_6[14]aneN_4)bpy]^{2+}$ [c]	19.3 (bun) ⟨4.5⟩{19.4 [2.6]}		13.97 (bun)	14.04 [0.89] (bun)	0.86 (1.47) (bun)	0.64 (bun)
$[Ru([14]aneN_4)bpy]^{2+}$ [b]	19.0 (d/w)	12.94 (d/w)	13.96 (d/w)	14.01 [0.95] (d/w)	0.85 (1.44) (d/w)	1.59 (d/w){22.8 (d/w)}
	19.5 (bun) ⟨5.0⟩{19.5 [2.3]}[c]	13.38 (bun)	13.99 (bun)	14.03 [0.89] (bun)	0.81 (1.45) (bun)	0.975 (bun){19.0 (bun)}
$[Ru([15]aneN_4)bpy]^{2+}$ [c]	19.3 (bun) ⟨4.5⟩{19.3 [2.0]}	13.15 (bun)	13.60 (bun)	13.63 [0.89] (bun)	0.78 (1.45) (bun)	3.1 (bun){25 (bun)}
$[Ru([12]aneN_4)bpy]^{2+}$ [c]	19.1 (bun) ⟨4.5⟩{19.5 [2.6]}		13.31 (bun)	13.37 [0.83] (bun)	0.48 (1.31) (bun)	0.39 (bun)
$[Ru(trien)bpy]^{2+}$ [c]	19.5 (bun) ⟨4.6⟩{19.5 [2.1]}	12.56 (bun)	13.00 (bun)	13.02 [0.87] (bun)	0.76 (1.43) (bun)	14 (bun)
$[Ru(en)_2bpy]^{2+}$ [b]	19.1 (d/w)	11.81 (d/w)	12.82 (d/w)	12.88 [1.03] (d/w)	0.85 (1.45) (d/w)	26 (d/w)
	19.2 (bun) ⟨4.7⟩{19.2 [2.1]}[c]	12.59 (bun)	13.01 (bun)	13.05 [0.89] (bun)	0.78 (1.45) (bun)	9.5 (bun)
$[Ru(NH_3)_4bpy]^{2+}$ [b]	18.9 (d/w)		12.02 (d/w)	12.09 [1.11] (d/w)	0.81 (1.45) (d/w)	39 (d/w)
	19.0 (bun) ⟨4.0⟩{19.0 [2.1]}[c]		12.37 (bun)	12.42 [0.92] (bun)	0.80 (1.48) (bun)	22 (bun)

[a] All energies in units of $cm^{-1}/10^3$. Abbreviations: d/w = DMSO/water; bun = butyronitrile. [b] Reference 28. [c] This work. [d] From the single-exponential fit of the luminescence decay.

independent and based on the ambient quantum yield, it contributes <15% to the $[Ru(bpy)_3]^{2+}$ [71] decay at 77 K, and this is probably an upper limit because the lowest-energy spin−orbit component of the ^{3}MLCT excited state for this complex has the lowest emission yield.[2]

Discussion

The mono(bipyridine) complexes examined here vary considerably in their emission energies, spectral band shapes, and lifetimes. Most remarkably, the complexes with 12-membered macrocyclic ligands, $[Ru([12]aneN_4)bpy]^{2+}$ and $[Ru([12]eneN_4)bpy]^{2+}$, have much longer 77 K excited-state lifetimes and smaller vibronic contributions to their band shapes than do other complexes with similar excited state−ground state energy differences. The variations observed in the spectral and kinetic properties are not simply correlated, and the ground-state structures of these macrocyclic ligand complexes indicate that for most of them the important stereochemical constraints are within the macrocyclic ligands and between these ligands and the Ru metal rather than between these ligands and the coordinated bpy. Thus, the Ru complex with a macrocyclic ligand in which stereochemical repulsions result in appreciable ground-state distortion of the bpy ligand has larger vibronic contributions to the band shape but a similar excited-state lifetime relative to comparable complexes, while the bpy ligand of $[Ru([12]aneN_4)bpy]^{2+}$ is not significantly distorted in the ground state. Overall, these complexes continue to exhibit considerable complexity of their MLCT excited states, and some of this may be a consequence of variations in excited state−excited state configurational mixing. Despite this complexity, or possibly because of it, it appears that relatively rigid "bystander" or "innocent" ligands can be used to increase the MLCT excited-state lifetimes of ruthenium poly(pyridine) MLCT excited states even when thermally activated processes do not play a significant role.

1. Structural Considerations. The pyridyl moieties of the coordinated bpy ligand are nearly coplanar with normal bond lengths and angles in the ground states of most complexes. Consequently, the determination that the MLCT excited-state

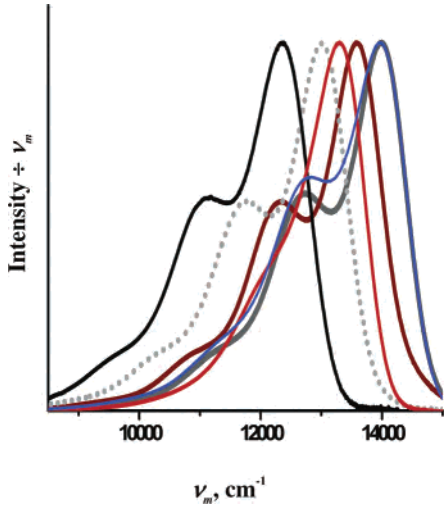

Figure 6. Emission spectra of the $[Ru(Am)_4bpy]^{2+}$ complexes at 77 K in butyronitrile glasses. Emission curves for Am equal to the following: $[14]aneN_4$, gray; $Me_6[14]aneN_4$, blue; $[15]aneN_4$, dark red; $[12]aneN_4$, red; $(en)_2$ and trien, gray dotted (there are some intensity differences in the 11500−12500-cm^{-1} region for these complexes); $(NH_3)_4$, black. The emission intensities are adjusted to 1.00.

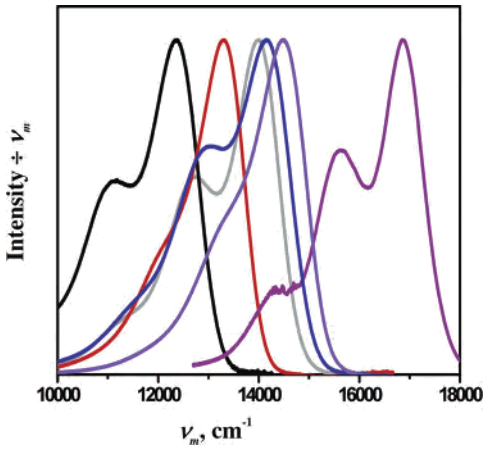

Figure 7. 77 K emission spectra of selected $[Ru(L)bpy]^{2+}$ complexes in butyronitrile glasses for L equal to the following: $(py)_4$, purple; $[14]aneN_4$, gray; $[12]aneN_4$, red; $[12]eneN_4$], violet; pyo$[12]eneN_4$, dark blue; $(NH_3)_4$, black. The maximum emission intensities are all adjusted to 1.00.

distortions of $[Ru(bpy)_3]^{2+}$ and $[Ru(NH_3)_4bpy]^{2+}$ involve displacements in the bpy ligand skeletal vibrational modes[30,31] implies different bond lengths, angles, and/or shapes of this ligand in the excited state. This is as expected for a $Ru^{II}bpy \rightarrow Ru^{III}bpy^-$ chromophore; however, the amplitudes of these displacements do not all vary in the systematic manner predicted by eq 3,[28] and the relatively large (and also variable) amplitudes of the displacements attributed to the Ru−N skeletal vibrational modes[30,31] are somewhat surprising because these appear to be less important in the thermal electron transfer.[26] Thus, the Ru−NH_3 bond lengths tend to be 4−6 pm longer in Ru^{II} than in Ru^{III} complexes, while the opposite ordering tends to be found for ruthenium pyridyl moieties,[72,73] and the variations in thermal self-exchange electron-transfer rates of Ru^{II}/Ru^{III} complexes appear to

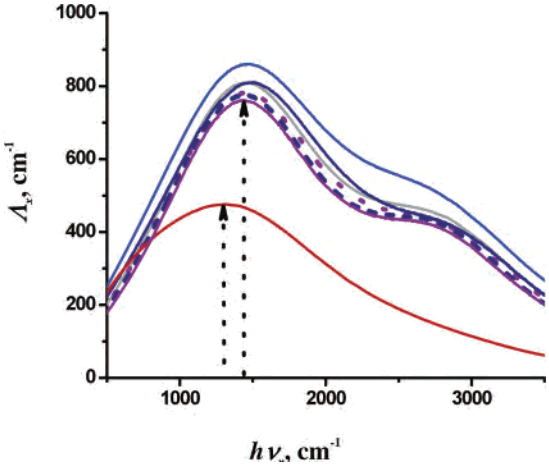

Figure 8. Reorganizational energy profiles for $[Ru(Am)_4bpy]^{2+}$ complexes for $(Am)_4$ equal to the following: $(Me_6[14]aneN_4)$, blue line; $(NH_3)_4$, dark-blue line; $[14]aneN_4$, solid gray line; $(en)_2$, purple dots; $[15]aneN_4$, dark-blue dashes; trien, purple line; $[12]aneN_4$, red line. The vertical arrows indicate the approximate maxima, $\Lambda_{x(max)}$, of $[Ru([12]aneN_4)bpy]^{2+}$ and the other $[Ru(Am)_4bpy]^{2+}$ complexes. The uncertainties in Λ_x are very large for $h\nu_x < 500$ cm^{-1} because the amplitudes of the fundamental and original emission spectra are comparable, as noted elsewhere.

depend largely on the variations in cation sizes and solvation energy differences;[26] e.g., for the $[Ru(bpy)_3]^{3+,2+}$ couple, the contribution of metal−ligand skeletal modes to λ_r is probably $\ll$80 cm^{-1}, while the rR study indicates that the sum of all vibrational reorganizational energies of the four MLCT excited-state displacement modes with $h\nu_k \leq 670$ cm^{-1} is $>\sim$200 cm^{-1},[30] about 60% of the comparable sum for $[Ru(NH_3)_4bpy]^{2+}$;[31] thus, it appears that different sets of Ru−N skeletal modes are involved in the thermal and excited-state processes. The ground-state range of Ru^{II}−N bond lengths in the structures reported here is roughly comparable to the range of reported Ru^{II}−N and Ru^{III}−N bond-length differences, but there is no clear overall correlation of the ground-state bond lengths with the differences in the excited-state lifetimes or the emission band shapes of these complexes.

On the other hand, the twisting of the bpy ligand in the ground state of the $[Ru(Me_6[14]aneN_4)bpy]^{2+}$ complex is very likely correlated with the larger vibronic contributions to the emission spectrum observed for this rather than for the related macrocyclic ligand complexes for distortion modes with $h\nu_k \approx 1500$ cm^{-1}, as illustrated in Figure 8. This is consistent with the expectation that the electron density in the bpy lowest unoccupied molecular order will tend to be equally distributed over both pyridyl moieties and that this is most consistent with the planarity around the 2,2′ linkage of the pyridyl moieties in the excited state. Obviously, any increase in the planarity of the bpy ligand in this complex is expected to be accompanied by displacement of the *gem*-methyl moieties and increased strain within the macrocyclic ligand, but the effects on the correlated first-order displacement modes (with $h\nu_k < \sim$1300 cm^{-1}) are not as evident in our observations (there may be a correlated higher-order contribution for $h\nu_x \approx 2400$ cm^{-1} in Figure 8).

2. Electrochemical−Optical Energy Correlations. The energies of the absorption maxima, $h\nu_{max(abs)}$, and the

(72) Richardson, D. E.; Walker, D. D.; Sutton, J. E.; Hodgson, K. O.; Taube, H. *Inorg. Chem.* **1979**, *18*, 2216.
(73) Shin, Y. K.; Szalda, D. J.; Brunschwig, B. S.; Creutz, C.; Sutin, N. *Inorg. Chem.* **1997**, *36*, 3190.

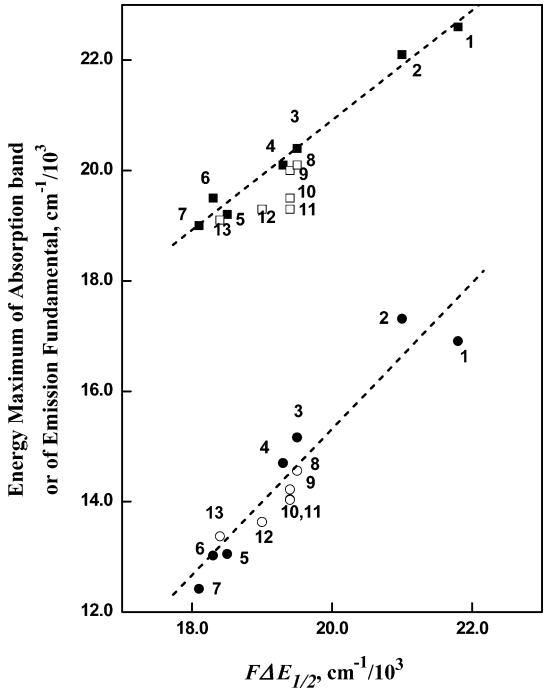

Figure 9. Correlation of differences between the oxidation and reduction half-wave potentials for $[Ru(L)bpy]^{2+}$ complexes with observed optical transition energies: upper data set for the lowest-energy MLCT absorption maximum; lower data set for the energy maximum of the fundamental component deconvoluted from the 77 K emission spectrum. Open rectangles and circles are for macrocyclic ligand complexes. L: $(py)_4$, 1; $(bpy)_2$, 2; (en)bpy, 3; $(NH_3)_2$bpy, 4; $(en)_2$, 5; trien, 6; $(NH_3)_4$, 7; [12]eneN_4, 8; pyo[14]-eneN_4, 9; Me_6[14]aneN_4, 10; [14]aneN_4, 11; [15]aneN_4, 12; [12]aneN_4, 13. The least-squares lines are calculated for the data points 1−7: slope = 0.99 ± 0.05 and intercept = 1 ± 1, top; 1.3 ± 0.2 and −11 ± 3, bottom.

emission fundamentals, $h\nu_{max(f)}$, correlate reasonably well with the differences between the half-wave potentials for the first oxidation and the first reduction of the complexes, as is shown in Figure 9 and expected for charge-transfer transitions.[19,74,75] Some of the macrocyclic ligand complexes deviate from the correlation line in Figure 9, and this may be a consequence of some differences in the variations of solvent reorganizational energies, λ_s, through this series of complexes. The contributions of λ_s to the fundamentals of the 77 K emission spectra should be very small because most of the solvent modes are expected to be frozen,[76] and all of the data points (except possibly for $[Ru(py)_4bpy]^{2+}$) are consistently near the correlation line in the plot of $h\nu_{max(f)}$ vs $F\Delta E_{1/2}$. The differences in the slopes of the correlations of absorption maxima and of $h\nu_{max(f)}$ with $F\Delta E_{1/2}$ probably arise mostly from the varying contributions of the exchange energy to the emission spectra [where the exchange energy is approximately $E^{00\prime}$(singlet) − $E^{0\prime 0}$(triplet) = $2K_{exch}$] because

$$h\nu_{max(abs)} \cong h\nu_{max(f)}(77\ K) + \lambda_s + 2K_{exch} \qquad (18)$$

The exchange energies are on the order of a few thousand

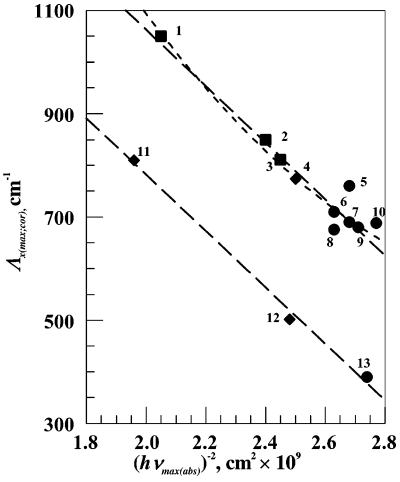

Figure 10. Variation of emrep amplitudes (corrected for bandwidth differences), $\Lambda_{x(max;cor)}$, with $(h\nu_{max(abs)})^{-2}$ for $[Ru(L)bpy]^{2+}$ complexes with L equal to the following: $(bpy)_2$, 1; en(bpy), 2; $(NH_3)_2$(bpy), 3; (pyo[14]-eneN_4), 4; (Me_6[14]aneN_4), 5; ([14]aneN_4), 6; ([15]aneN_4), 7; trien, 8; $(en)_2$, 9; $(NH_3)_4$, 10; $(py)_4$, 11; ([12]eneN_4), 12; ([12]aneN_4), 13. The best-fit curves for the top set of data points are (large dashes) $\Lambda_{x(max;cor)} = 2200 \pm 100 - (550 \pm 40) \times 10^9\ [(h\nu_{max(abs)})^{-2}]$ and (small dashes) $\Lambda_{x(max;cor)} = 3800 \pm 900 - (1900 \pm 700) \times 10^9\ [(h\nu_{max(abs)})^{-2}] + (280 \pm 150) \times 10^{18}\ [(h\nu_{max(abs)})^{-4}]$. For the lower data set: $\Lambda_{x(max;cor)} = 1900 \pm 100 - (550 \pm 40) \times 10^9\ [(h\nu_{max(abs)})^{-2}]$.

wavenumbers for these complexes, apparently much larger for $[Ru(NH_3)_4bpy]^{2+}$ than for $[Ru(bpy)_3]^{2+}$ [15] and probably not the same for all of the tetraam(m)ine complexes. While the absorption energy maxima appear to vary in roughly a 1:1 manner with $F\Delta E_{1/2}$, this may be deceptive because (a) the absorption maxima are functions of the component bandwidth (due to the overlap of vibronic components and the fundamentals; see the discussion above and Figure 10 in Xie et al.[28]), (b) the species involved in the electrochemical and optical processes are different,[17,75] and (c) configurational mixing among excited states may be an issue affecting $E^{00\prime}$ (see below). Because configurational mixing increases the energy differences between the electronic states[19] and because the emission energies are smaller than the absorption energies, correction for the effects of configurational mixing on the excited-state energies will increase the contrast in the slopes for absorption and emission data in Figure 9.

3. Attenuation of Reorganizational Energies and Configurational Mixing of the ^{3}MLCT Excited State with the Ground State. For correlations of the experimental data, it is useful to recast eq 2 as

$$\Lambda_{x(max)} \cong \Lambda_{x(max)}^{\circ}(1 - n_e\alpha_{eff}^{\ 2}) \cong \Lambda_{x(max)}^{\circ} - n_e\frac{H_{eff}^{\ 2}}{(h\nu_{max(abs)})^2}\Lambda_{x(max)}^{\circ} \qquad (19)$$

Such a correlation is presented in Figure 10, and as previously observed,[28] it illustrates the very strong attenuation of vibrational reorganizational energies that results from the configurational mixing of the ground and MLCT excited states. The values of $\Lambda_{x(max)}$, plotted in Figure 10, correspond to the sums of the reorganizational energy contributions (first and second order) near $h\nu_x = 1490\ cm^{-1}$ for all complexes except for the complexes with $(L)_4$ = [12]aneN_4 and

(74) Endicott, J. F. In *Electron Transfer in Chemistry*; Balzani, V., Ed.; Wiley-VCH: New York, 2001; Vol. 1; p 238.
(75) Lever, A. B. P.; Dodsworth, E. In *Electronic Structure and Spectroscopy of Inorganic Compounds*; Lever, A. B. P., Solomon, E. I., Eds.; Wiley: New York, 1999; Vol. II, p 227.
(76) Marcus, R. A. *J. Phys. Chem.* **1990**, *94*, 4963.

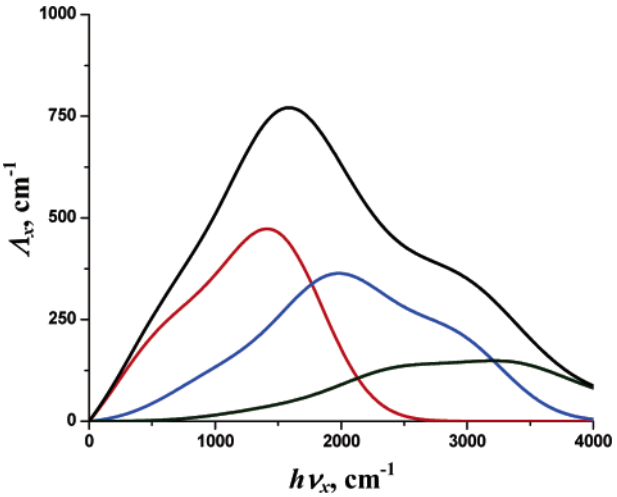

Figure 11. Emrep contributions calculated from rR parameters reported for $[Ru(NH_3)_4bpy]^{2+}$ [26] using eqs 9−15. The first-order emrep components (red) were based on eq 11, the second-order components (blue) on eq 12, and the third-order components (green) on eq 13. The solid black curve is the calculated emrep = sum of the three components (see Figure 6 in Xie et al.[28]). The fundamental component used in eq 9 was that deconvoluted from the experimental emission spectrum using Grams32.

[12]eneN$_4$, for which $h\nu_x = 1340$ cm^{-1} (see Table 5), and the principal first-order contributions in this region are bpy skeletal modes.[30,31,77] On the other hand, the second-order contributions in this region will arise mostly from contributions of Ru−ligand skeletal modes (e.g., see Figure 11).

We use the energy of the absorption maximum, $h\nu_{max(abs)}$, in eq 19 because most of this attenuation arises from the shifts of the PE minima and because H_{ge} is probably larger than H_{eg} (for the singlet and triplet states, respectively).[78] That the complexes represented by data points 1−10 in Figure 10 appear to be correlated with a single value of Λ_x° is consistent with the model of a simple Ru−bpy chromophore whose excited-state energy is altered by the ligands L and in which these ligands make no other significant contributions to the properties of the MLCT excited state. There is considerable scatter of data points 5−10 around the correlation line, and because these are the complexes with the smallest values of $h\nu_{max(abs)}$, this scatter may arise from some combination of factors: (a) the relatively large value of $\Lambda_{x(max)}$ for $[Ru(Me_6[14]aneN_4)bpy]^{2+}$ is consistent with the observed twist of the bpy ligand in the ground-state structure, as discussed above; (b) eqs 3 and 19 are only valid for weak configurational mixing, $\alpha_{jk}^2 < 0.1$, and this is unlikely to be the case for complexes with the smallest values of $h\nu_{max(abs)}$;(c) in view of eq 19 and the large and differing contributions of K_{exch}, the α_{eg}^2 term of eq 4 may make different contributions through the series of complexes (not accommodated in our use of $h\nu_{max(abs)}$). The curved correlation line in Figure 10 is a simple means for evaluating the significance of higher order contributions to eqs 4 and 19, but apparently including terms on the order of α_{jk}^4 does not improve the fit to the experimental data.

(77) Stromen, D. P.; Mallick, P. K.; Danzer, G. D.; Lumpkin, R. S.; Kincaid, J. R. *J. Phys. Chem.* **1990**, *94*, 1357.
(78) Coe, B. J.; Harris, J. A.; Brunschwig, B. S.; Asselberghs, I.; Clays, K.; Garin, J.; Orduna, J. *J. Am. Chem. Soc.* **2005**, *127*, 13399.

However, Figure 10 demonstrates clearly that vibronic contributions to the emission spectra of the $[Ru(py)_4bpy]^{2+}$, $[Ru([12]eneN_4)bpy]^{2+}$, and $[Ru([12]aneN_4)bpy]^{2+}$ complexes are much smaller than those of the other complexes with comparable excited-state energies (or comparable $h\nu_{max(abs)}$), and the preceding section has established that there is nothing anomalous about the excited-state energies of these complexes (although the energy of the ^{3}MLCT excited state of $[Ru(py)_4bpy]^{2+}$ may be somewhat lower than expected based on the electrochemical correlation). This considerable attenuation of vibronic sidebands (by about 300 cm^{-1} or 30−40% in $\Lambda_{x(max)}$) must arise from smaller distortions in some combination of vibrational modes in the MLCT excited states of these complexes in the absence of configurational mixing with the ground state. We have used the emrep maxima in the correlations shown in Figure 10, and there are several important points that must be considered in interpreting the observed effects: (a) these maxima are shifted to slightly smaller vibrational energies for $[Ru([12]eneN_4)bpy]^{2+}$ and $[Ru([12]aneN_4)bpy]^{2+}$ than for the other complexes ($h\nu_x \sim 1300$ cm^{-1} compared to ~1450 cm^{-1}); (b) the amplitudes of the emrep maxima are much larger than the vibrational reorganizational amplitudes of the individual distortion modes when the vibrational energy differences are small compared to the component bandwidth;[38] and (c) there are significant second-order contributions to the emrep amplitudes in the $h\nu_x = 1300-1500$-cm^{-1} range,[28] as is illustrated for $[Ru(NH_3)_4bpy]^{2+}$ in Figure 12. Our attempts to simulate the $[Ru([12]aneN_4)bpy]^{2+}$ emrep by varying the rR parameters reported for $[Ru(NH_3)_4bpy]^{2+}$ [31] indicate that some combination of strongly attenuated bpy skeletal (1300−1600 cm^{-1}) and low-frequency (500−1000 cm^{-1}) vibronic terms is required for a reasonable fit of the spectrum. The unusually weak vibronic sidebands observed for the $[Ru(py)_4bpy]^{2+}$, $[Ru([12]eneN_4)bpy]^{2+}$, and $[Ru([12]aneN_4)bpy]^{2+}$ complexes appear to be a property of the electronic excited states. This surprising contrast in the distortions of the nominally Ru−bpy MLCT electronic excited states could arise from differences in the effects of configurational mixing with a slightly higher-energy, highly distorted electronic excited state. A ligand-field triplet excited state (^{3}LF) of Ru^{II} is one possible candidate for such a state.

4. Expected Effects on Reorganizational Energies and Vibronic Sidebands of ^{3}MLCT Excited-State Configurational Mixing with Other Electronic Excited States. The observations described above raise several issues. Thus, if the "extra" attenuation of the vibronic sidebands observed for $[Ru(py)_4bpy]^{2+}$, $[Ru([12]eneN_4)bpy]^{2+}$, and $[Ru([12]aneN_4)bpy]^{2+}$ relative to the other complexes arises from different effects of the configurational mixing, then (a) which electronic states are likely to be involved, (b) how should the configurational mixing between excited states be manifested in the intensities of the vibronic components, and (c) is there a plausible mechanism for the observed variations of band shapes?

As noted in Figure 1, the nearest in energy electronic states that might mix with the ^{3}MLCT excited state are an internal ligand (IL or $\pi\pi^*$ excited state of bpy) and a LF excited

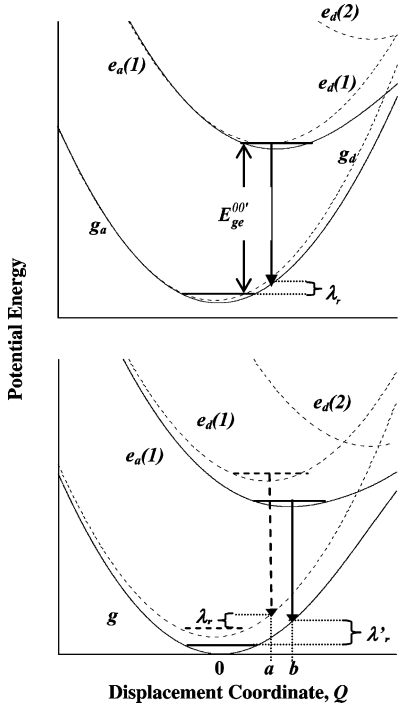

Figure 12. Qualitative PE curves illustrating the effects of configurational mixing between two excited states [e(1) and e(2)] with different nuclear distortions [$Q_{min(1)} < Q_{min(2)}$] on the observed reorganizational energy, λ_r, when the excited-state PE minima are similar (bottom) and appreciably different (top) in energy. When the energy differences are large, the diabatic (d) and adiabatic (a) PE curves are similar near the excited-state minimum (top); it is assumed that both excited states mix with the ground state, and the reorganizational energy from the top panel is entered in the bottom panel to illustrate an increase of the reorganizational energy with increased excited-state mixing ($\lambda_r' > \lambda_r$). Note that the relationship between the zero-point-energy differences of the diabatic and adiabatic states, $E_{ge(d)}^{00'}$ and $E_{ge(a)}^{00'}$, in the three-state system depends on the relative extents of the mixing of the lowest-energy excited state with the ground state and with the upper excited state.

state (the higher-energy MLCT excited states in Figure 1 are presumed to be adiabatic states, already mixed into the lowest-energy state).[16,18] If the higher-energy excited state is more distorted along some nuclear coordinate than is the diabatic MLCT excited state, then one expects configurational mixing of the excited states to increase the distortion of the MLCT excited state along this coordinate, as is illustrated in Figure 12. The ^{3}IL state is expected to be similar in energy through the series of complexes, and the observation of much weaker vibronic sidebands in $[Ru(py)_4bpy]^{2+}$ than in $[Ru(bpy)_3]^{2+}$, despite their similar emission energies, indicates that this state would not readily account for the observations.

While no ^{3}LF excited state of the Ru^{II} complexes has been identified, $[Rh(NH_3)_6]^{3+}$, which is isoelectronic with $[Ru(NH_3)_6]^{2+}$, has a broad ^{3}LF ($^3T_{1g}$) emission band centered at about 17 000 cm^{-1} with an origin at about 21 000 cm^{-1}.[20] This band is attributed to vibronic progressions in the Rh−N O_h skeletal a_{ig} (500 cm^{-1}) and e_g (480 cm^{-1}) vibrational modes in which the excited state is so distorted that the Huang−Rhys parameters are estimated to be $S_{a_{1g}} \cong 0.6$ and $S_{e_g} \cong 14$;[20] the latter is nearly 50 times larger than the largest value of S_k inferred from rR spectra of either $[Ru(bpy)_3]^{2+}$ [30] or $[Ru(NH_3)_4bpy]^{2+}$.[31] The lower charge of Ru^{II} is expected to result in a lower energy and probably somewhat smaller distortion of the comparable state in $[Ru(NH_3)_6]^{2+}$; thus, the lowest-energy LF absorptions of these complexes have their maxima at about 32 500 and 26 500 cm^{-1}, respectively (see also Figure 1).[14,20] If this energy difference is the same for the ^{3}LF excited states, then the ^{3}LF state of $[Ru(NH_3)_6]^{2+}$ should have its origin in the 15 000−17 000-cm^{-1} energy range. The energies of the LF states are determined largely by the electronic pairing energy and the energy differences of the d_σ and d_π orbitals, or $10Dq \cong 3\sigma_L - 4\pi_L$, where σ_L and π_L are the respective orbital energy parameters of the angular overlap model (the values tabulated for these parameters are determined with respect to the ground-state nuclear coordinates).[14,79,80] The σ_L parameters are usually approximately the same for the am(m)ine and pyridyl ligands, but the π_L parameters, usually taken as zero for am(m)ines, are found to be significantly negative for pyridyl ligands.[79,80] For example, the π_L parameter (per N) for $[Cr(bpy)_3]^{3+}$ has been found to be −250 cm^{-1},[81] and the π_L parameter for $[Ru(bpy)_3]^{2+}$ should be more negative. In any case, the ^{3}LF state energies are only a few thousand wavenumbers larger than the ^{3}MLCT energies and the ^{3}LF excited-state energies may approximately track the variations of the ^{3}MLCT energies in the $[Ru(Am)_{6-2n}(bpy)_n]^{2+}$ complexes due to an increase in the π_L contributions as the number of bpy ligands increases. The tetragonally distorted $^3T_{1g}$ excited state of the octahedral complexes,[20] mentioned above, will split into two or more components in the low-symmetry complexes discussed in this paper, and each of these components will be distorted with respect to the ground-state metal−ligand normal coordinates. Thus, configurational mixing with this electronic excited state is expected to result in an increase in the metal−ligand distortion of a ^{3}MLCT excited state, as illustrated in Figure 12.

The configurational mixing among electronic excited states that tends to increase some distortion coordinates so that $\Delta Q_k[e_d(2)] > \Delta Q_k[e_d(1)]$ for the distortions of the lowest energy of the excited states, and this can be described by a relatively simple perturbation theory argument. Thus, for the vibronic contributions represented in terms of the differences in the distortion coordinate, Q_k, for the PE minima of the electronic ground and lowest-energy excited states, and for two excited states, $Q_{k(0)}$ and $Q_{k(0')}$, respectively, the attenuation of the reorganizational energies for this coordinate in eqs 3 and 19 that arises because the $Q_k < Q_{k(0)}$ when configurational mixing is important must be modified as in (details in the Supporting Information)[63]

$$\lambda_k \approx \lambda_{k(0)}\left(1 - 2\alpha_{ge}^{\ 2} - 2\alpha_{eg}^{\ 2} + 2\alpha_{ee'}^{\ 2}\sqrt{\frac{\lambda_{k(0')}}{\lambda_{k(0)}}}\right)_k \quad (20)$$

The $(2\alpha_{ee'}^{\ 2}\sqrt{\lambda_{k(0')}/\lambda_{k(0)}})_k$ term in eq 20 arises from excited state−excited state configurational mixing and the shift of

(79) Figgis, B. N.; Hitchman, M. A. *Ligand Field Theory and its Applications*; Wiley-VCH: New York, 2000.
(80) Vanquickenbourne, L. G.; Ceulemans, A. *Coord. Chem. Rev.* **1983**, *100*, 157.
(81) Ryu, C. K.; Endicott, J. F. *Inorg. Chem.* **1987**, *27*, 2203.

the PE minimum of the lowest-energy excited state (e) along a coordinate in which the upper excited state (e′) is more distorted; the reorganizational parameters $\lambda_{k(0)}$ and $\lambda_{k(0')}$ are defined with respect to the difference in the PE minima of the two excited states along the distortion coordinate Q_k (additional details are given in the Supporting Information).[63] Equation 20 illustrates how increased configurational mixing among excited states can increase the distortion of some coordinates and thereby the vibronic sideband intensity.

The distortions expected of the ^{3}LF excited state[20,82] (as in $[Rh(NH_3)_6]^{3+}$; see the above discussion) and the relatively small vibronic sideband intensities observed for the $[Ru(py)_4bpy]^{2+}$, $[Ru([12]eneN_4)bpy]^{2+}$, and $[Ru([12]aneN_4)bpy]^{2+}$ complexes (Figure 10) suggest that less LF excited-state character is mixed into the ^{3}MLCT excited states of these complexes. Less ^{3}LF/^{3}MLCT mixing for these complexes than for the $[Ru(NH_3)_{2n-6}(bpy)_n]^{2+}$ complexes corresponds to a smaller contribution of the $[2\alpha_{ee'}^2\sqrt{\lambda_{k(0')}/\lambda_{k(0)}}]_k$ term for the former than for the latter complexes. This could be the result of either (a) relatively small values of $\alpha_{ee'}^2$ (this would be the case for significantly larger values of the vertical energy difference $E_{ee'}$) or (b) a very small difference in the PE minima of the excited states along the distortion coordinate. It is possible that $E_{ee'}$ is larger for $[Ru(py)_4bpy]^{2+}$ than for $[Ru(bpy)_3]^{2+}$ (note there are different angular overlap and orbital phase issues involved for these complexes), but we have no experimental information bearing on this point.

Because there is very little stereochemical flexibility in the coordination of the $[12]aneN_4$ and $[12]eneN_4$ ligands, it is likely that the difference in the PE minima of the MLCT and LF excited states along the distortion coordinate is relatively small. If this is the case, one would expect $E_{ee'}^{0'0''}$ and the force constants (for the distortion mode) to be somewhat larger for these than for the other complexes. This argument is qualitatively consistent with the observations that the lowest-energy LF absorption bands are somewhat similar in energy for the corresponding *cis*-$[Co^{III}(Am)_4X_2]^{n+}$ complexes,[83−85] despite the tendency of the LF excited state to distort[20,82] and the stereochemical constraints on coordination-sphere distortion imposed by the $[12]aneN_4$ ligand; see Table S1 in the Supporting Information.[63]

5. Effects of Variations in the "Innocent" Ligands on the 77 K ^{3}MLCT Excited-State Lifetimes. The 77 K excited-state lifetime of $[Ru([12]aneN_4)bpy]^{2+}$ is 36 times longer than that of $[Ru(trien)bpy]^{2+}$ despite their nearly identical values of $h\nu_{max(f)}$. These two tetraamine ligands differ only in an ethylene moiety linking two of the amines, and this, as well as the contrast in the band shapes, is a striking example of alteration of the properties of the Ru−bpy MLCT excited state by means of simple structural changes in the nonchromophoric (or "innocent") ligands.

The rate constant for nonradiative excited-state relaxation is well established to decrease with increasing ground state−excited state energy differences;[4,7,8,12,24,39−42,86−90] thus, in the low-temperature frozen media limit appropriate to this work, for weak electronic coupling between the two states and for a single coupled vibrational mode *h*, the relationship can be expressed as in eq 4.[39] Because it appears that the highest-frequency C−H and N−H stretching modes have vibrational reorganizational energies that are too small ($\lambda_{CH} \ll 30$ cm^{-1} and $\lambda_{NH} \ll 10$ cm^{-1})[33] for the relaxation to be dominated by a channel corresponding to a harmonic of only one of these vibrational modes, thus for such a single-mode contribution, $\gamma_{RH} > 5$ and $k_{nr(obsd)} \div k_{nr(calcd)} \gg 10^4$ based on eq 4. Although the bpy skeletal modes appear to contribute most to the vibronic sidebands, the largest vibrational reorganizational energies of these modes are found for the vibration at about 1490 cm^{-1} with $\lambda_h \cong 400$ cm^{-1} (for $[Ru(bpy)_3]^{2+}$)[30] and $\lambda_h \cong 225$ cm^{-1} (for $[Ru(NH_3)_4bpy]^{2+}$),[31] and for this vibrational mode $E^{0'0}/h\nu_h > 8$ and $\gamma_h > 2.75$; thus, $k_{nr(calcd)}$ based on this mode alone is even smaller than that found above for the C−H modes. However, this use of eq 21 to estimate the rate constant for the isoenergetic crossing from ^{3}MLCT to the ground state presumes that the crossing only populates a higher harmonic, based on the values of the ratio $E^{0'0}/h\nu_h$, of a fundamental distortion mode; however, the large number of distortion modes for these complexes (more than 11)[30,31] suggests that there are a very large number of possible relaxation channels, each of which can be represented by the sum of a different combination of distortion modes; i.e., corresponding to the frequencies $n_1\nu_1$, $n_2\nu_2$, $n_3\nu_3$, $n_4\nu_4$, ... such that $\sum_k n_k\nu_k \approx E^{0'0} \pm k_BT$. The discrepancies noted above suggest that a sum over 10^4-10^6 different relaxation channels (*h*) would be required to account for the observed rate constants, but even if only eight of the distortion modes contribute to the relaxation channels and $\sum_k n_k \approx 8$, there are still more than 4×10^4 possible combinations of these modes. Because some of the larger vibrational reorganizational energies found in the rR studies are for Ru−ligand skeletal modes,[30,31] such low-frequency modes could contribute to some of these relaxation channels, and such contributions seem to be required to account for the CH/CD and NH/ND isotope effects.[33] It is these Ru−ligand skeletal vibrational modes that should be most affected by configurational mixing between the ^{3}LF and ^{3}MLCT excited states. However, the large-amplitude distortion that is characteristic of the $^3T_{1g}(O_h)$ excited state[20,82] could couple with a large distortion of the bpy ligand in some normal vibrational modes of the complex.

Conclusions

A systematic comparison of $[Ru(L)_4bpy]^{2+}$ complexes has demonstrated that the vibronic contributions to their emission band shapes and excited-state lifetimes can be significantly altered by both (a) changes in the vertical energy difference

(82) Wilson, R. B.; Solomon, E. I. *J. Am. Chem. Soc.* **1980**, *102*, 4085.
(83) Collman, J. P.; Schneider, P. W. *Inorg. Chem.* **1966**, *5*, 1380.
(84) Hung, Y.; Martin, L. Y.; Jackels, S. C.; Tait, A. M.; Busch, D. H. *J. Am. Chem. Soc.* **1977**, *99*, 4029.
(85) Tsintavis, C.; Li, H.-L.; Chambers, J. Q.; Hobbs, D. T. *J. Phys. Chem.* **1991**, *95*, 289.
(86) Newton, M. D.; Sutin, N. *Annu. Rev. Phys. Chem.* **1984**, *35*, 437.
(87) Marcus, R. A. *Discuss. Faraday Soc.* **1960**, *29*, 21.
(88) Marcus, R. A.; Sutin, N. *Biochim. Biophys. Acta* **1985**, *811*, 265.
(89) Marcus, R. A. *Annu. Rev. Phys. Chem.* **1964**, *15*, 155.
(90) Richardson, D. E. In *Inorganic Electronic Structiure and Spectroscopy*; Solomon, E. I., Lever, A. B. P., Eds.; Wiley: New York, 1999; Vol. II.; p 131.

between the ground and excited electronic states and (b) relatively small structural changes in the nonchromophoric ligands. The intensities of the vibronic sidebands systematically decrease as the energy difference between the states decreases (e.g., over about a 2-fold range for $[Ru(NH_3)_{6-2n}(bpy)_n]^{2+}$ complexes), and this is an expected consequence of MLCT excited state−ground state configurational mixing. More surprising were the 40% smaller vibronic intensity and the 36-fold longer lifetime of $[Ru([12]aneN_4)bpy]^{2+}$ than of the closely related $[Ru(trien)bpy]^{2+}$ complex [these contrasts are notable because these complexes have nearly the same emission energies and differ structurally by only one ethylene linkage of the $(L)_4$ ligand] and the very similar "extra" attenuations of vibronic sideband intensities found for $[Ru([12]eneN_4)bpy]^{2+}$ and $[Ru(py)_4bpy]^{2+}$. That the three complexes that exhibit the unusually weak vibronic sidebands also exhibit the expected attenuation of their sideband amplitudes with the vertical energy difference between the MLCT excited state and the ground state indicates that they lack some distortional contribution(s) that is (are) common to the MLCT excited-state distortions in most $[Ru(L)_4bpy]^{2+}$ complexes. The observed behavior is not consistent with simple models of the MLCT excited state (e.g., two-state Ru−bpy chromophore or single distortion mode models). The relative stereochemical rigidity of the $[12]aneN_4$ ligand, which could reduce the amplitudes of distortions in some normal vibrational modes of the Ru−ligand coordination sphere, suggests that the distortional contribution that is missing in the MLCT excited state of the $[Ru([12]aneN_4)bpy]^{2+}$ complex arises from configurational mixing with a higher-energy LF excited state. Such configurational mixing will combine some of the properties of the LF excited state into the MLCT excited state as well as alter the relative energies of these excited states. Among the expected consequences of this mixing are increased distortions in the Ru−N skeletal modes in the MLCT excited state, and this is reasonably consistent with our observations. Thus, stereochemical changes in the nonchromophoric ligands that are expected to limit the amplitude of the LF excited-state distortions, thereby increasing the ^{3}LF−^{3}MLCT zero-point-energy differences and decreasing the distortion of the LF excited state, do alter the properties of the ^{3}MLCT excited state. On the other hand, the comparisons of the reorganizational energy profiles of these and the $[Ru(NH_3)_{6-2n}(bpy)_n]^{2+}$ complexes also appear to implicate changes in some first-order distortion modes that have higher frequencies than the Ru−N vibrational modes. However, the interpretation of these observations is complicated by such features of these molecules as (a) the significant contributions of second-order vibronic components to the band shape in the $h\nu_x \approx 1300-1600$-cm^{-1} range (see Figure 8) and (b) the fact that the normal vibrational modes are molecular, not independent bpy and metal−ligand skeletal modes, so that it is likely that some of the normal vibrational modes with frequencies in the 1300−1650-cm^{-1} range contain appreciable metal−ligand skeletal contributions.

Stereochemical manipulation of the properties of the electronic excited states of Cr^{III} complexes has also been demonstrated,[91−93] but in those complexes, the stereochemical constraints were designed to either promote or inhibit a thermally activated trigonal twist of the lowest-energy excited state. In contrast, the stereochemical constraints that alter excited-state lifetimes of the Ru^{II} complexes discussed here appear to be those that inhibit a tetragonal distortion of a higher-energy excited state, and the effect on the lowest-energy excited state lifetimes appears to be the consequence of configurational mixing between excited states rather than thermally activated population of the upper state. While this contrasts to the thermally promoted population of a higher-energy LF state such as has been proposed to account for ambient MLCT excited-state lifetimes and the chemistry of some Ru^{II} complexes,[94−97] these previous proposals do require a relatively low-energy LF excited state, and in this sense the mechanisms proposed to account for the ambient behavior and the 77 K spectral band shapes are consistent. The important effects reported here are large changes in the intensities of the vibronic sidebands of the MLCT emission spectra and thus the variations in excited-state molecular structure and their effects on excited-state lifetimes. Although the details of the stereochemical manipulation of excited-state lifetimes in Ru^{II} and Cr^{III} complexes differ, in both cases the effectiveness of the approach appears to depend on the small energy differences between the electronic excited states of the complexes and on the sensitivity of LF excited states to differences in their coordination environments.

Acknowledgment. The authors thank the Office of Basic Energy Sciences of the Department of Energy for partial support of this research.

Supporting Information Available: CIF files, table of Co^{III} and Rh^{III} LF absorption data, differential pulsed polarigram of $[Ru([12]aneN_4)bpy]^{2+}$, possible structure of $[Ru(pyo[14]eneN_4)bpy]^{2+}$, and an approach to three-state configurational mixing. This material is available free of charge via the Internet at http://pubs.acs.org.

IC0602547

(91) Lessard, R. B.; Heeg, M. J.; Buranda, T.; Perkovic, M. W.; Schwarz, C. L.; Rudong, Y.; Endicott, J. F. *Inorg. Chem.* **1992**, *31*, 3091.
(92) Perkovic, M. W.; Heeg, M. J.; Endicott, J. F. *Inorg. Chem.* **1991**, *30*, 3140.
(93) Endicott, J. F.; Perkovic, M. W.; Heeg, M. J.; Ryu, C. K.; Thompson, D. In *Electron-Transfer Reactions: Inorganic, Organometallic and Biological Applications*; Isied, S. S., Ed.; American Chemical Society: Washington, DC, 1997; Vol. 253; p 199.
(94) Ford, P. C. In *Inorganic and Organometallic Photochemistry*; Wrighton, M. S., Ed.; American Chemical Society: Washington, DC, 1978; Vol. 168; p 73.
(95) Maruszewski, K.; Stromen, D. P.; Kincaid, J. R. *J. Am. Chem. Soc.* **1993**, *115*, 8345.
(96) Maruszewski, K.; Kincaid, J. R. *Inorg. Chem.* **1995**, *34*, 2002.
(97) Sykora, M.; Kincaid, J. R. *Inorg. Chem.* **1995**, *34*, 5852.